


RESEARCH

Open Access

m⁶A modification suppresses ocular melanoma through modulating *HINT2* mRNA translation



Ruobing Jia^{1,3†}, Peiwei Chai^{1,3†}, Shanzheng Wang^{2,4†}, Baofa Sun^{2,4,5}, Yangfan Xu^{1,3}, Ying Yang^{2,4,5} , Shengfang Ge^{1,3}, Renbing Jia^{1,3*}, Yun-Gui Yang^{2,4,5*} and Xianqun Fan^{1,3*}

Abstract

Background: Dynamic N⁶-methyladenosine (m⁶A) RNA modification generated and erased by N⁶-methyltransferases and demethylases regulates gene expression, alternative splicing and cell fate. Ocular melanoma, comprising uveal melanoma (UM) and conjunctival melanoma (CM), is the most common primary eye tumor in adults and the 2nd most common melanoma. However, the functional role of m⁶A modification in ocular melanoma remains unclear.

Methods: m⁶A assays and survival analysis were used to explore decreased global m⁶A levels, indicating a late stage of ocular melanoma and a poor prognosis. Multiomic analysis of miCLIP-seq, RNA-seq and Label-free MS data revealed that m⁶A RNA modification posttranscriptionally promoted *HINT2* expression. RNA immunoprecipitation (RIP)-qPCR and dual luciferase assays revealed that *HINT2* mRNA specifically interacted with YTHDF1. Furthermore, polysome profiling analysis indicated a greater amount of *HINT2* mRNA in the translation pool in ocular melanoma cells with higher m⁶A methylation.

Results: Here, we show that RNA methylation significantly inhibits the progression of UM and CM. Ocular melanoma samples showed decreased m⁶A levels, indicating a poor prognosis. Changes in global m⁶A modification were highly associated with tumor progression in vitro and in vivo. Mechanistically, YTHDF1 promoted the translation of methylated *HINT2* mRNA, a tumor suppressor in ocular melanoma.

Conclusions: Our work uncovers a critical function for m⁶A methylation in ocular melanoma and provides additional insight into the understanding of m⁶A modification.

Keywords: m⁶A, Melanoma, *HINT2*, Translation, Tumorigenesis

* Correspondence: renbingjia@sjtu.edu.cn; ygyang@big.ac.cn; fanxq@sjtu.edu.cn

[†]Ruobing Jia, Peiwei Chai and Shanzheng Wang contributed equally to this work.

¹Department of Ophthalmology, Ninth People's Hospital, Shanghai JiaoTong University School of Medicine, Shanghai 20025, People's Republic of China

²Key Laboratory of Genomic and Precision Medicine, Collaborative Innovation Center of Genetics and Development, Beijing Institute of Genomics, Chinese Academy of Sciences, Beijing 100101, China

Full list of author information is available at the end of the article



Background

N⁶-Methyladenosine (m⁶A), the most prevalent modification in mRNA [1, 2], is a dynamic RNA modification installed by “writer” methyltransferase-like 3 (METTL3), methyltransferase-like 14 (METTL14) and Wilms tumor associated protein (WTAP) [3–5]; erased by “eraser” fat-mass and obesity-associated protein (FTO) and α -ketoglutarate-dependent dioxygenase alkB homolog 5 (ALKBH5) [6, 7]; and recognized by “readers”. Dynamic m⁶A modification affects a variety of cellular processes, such as RNA stability, export, splicing or translation [2]. For instance, m⁶A modification promotes the degradation of *Notch1a* mRNA in the earliest hematopoietic progenitor cells [3] while promoting the translation of immediate-early genes in long-term memory [8]. Therefore, m⁶A RNA modifications have attracted increasing attention in the pathogenesis of human disease.

As m⁶A modifications play a key role in the maintenance of homeostasis, aberrant m⁶A modifications may be an important inducer of tumorigenesis [2]. Disturbance of m⁶A modifications was reported to contribute to the tumorigenesis of glioblastoma, breast cancer and hepatocellular carcinoma [9]. For example, decreased *METTL3* expression or *METTL14* mutation in endometrial cancer reduces the m⁶A modification of AKT pathway-related genes, resulting in the activation of the AKT signaling pathway and contributing to tumorigenesis [10]. In addition, FTO erases m⁶A modification of tumor suppressor genes *MYC/CEBPA*, which contributes to the tumor formation of leukemia. Therapeutically, R-2-hydroxyglutarate inhibits the activity of FTO, thereby suppressing leukemia progression. Thus, exploration of the novel m⁶A RNA methylation drivers of tumorigenesis is potentially interesting.

Ocular melanoma, including uveal melanoma (UM) and conjunctival melanoma (CM), is the most common primary eye tumor in adults and the 2nd most common melanoma, with a high rate of recurrence and poor prognosis [11–13]. The loss of one copy of chromosome 3 has been frequently identified in ocular melanoma. Previous studies have revealed that mutations in G protein subunit alpha Q (GNAQ) or G protein subunit alpha 11 (GNA11) result in the promotion of cell proliferation and sensitize cells to mitogen-activated protein kinase (MAPK) inhibitors. Furthermore, epigenetic drivers, such as DNA methylation, histone modifications, microRNAs and lncRNAs, also participate in tumorigenesis of ocular melanoma [14–16]. For instance, lncRNA *ROR* serves as a decoy oncoRNA that blocks G9a (a key enzyme of histone methylation) binding to the surfaces of target DNA, thereby promoting UM tumorigenesis, while

lncRNA *CASC15-New-Transcript 1 (CANTI)* inhibits UM progression by simultaneously activating other lncRNAs, *JPX* and *FTX*. However, the functional role of dynamic tuning of m⁶A in ocular melanoma tumorigenesis remains unclear.

We thus aimed to identify the functional role of m⁶A methylation in malignant ocular melanoma and reveal its potential mechanism in tumorigenesis. We show that m⁶A methylation significantly inhibits the progression of ocular melanoma cells. Mechanistically, m⁶A methylation recognized by YTH N⁶-methyladenosine RNA binding protein 1 (YTHDF1) promotes translation of histidine triad nucleotide-binding protein 2 (*HINT2*), a tumor suppressor in ocular melanoma. Our study reveals the functional importance of RNA m⁶A methylation and thereby presents a novel dynamic mechanism of m⁶A RNA modifications.

Methods

Patient samples

A total of 88 human ocular melanoma tissues and 28 human normal melanocyte tissues were collected for immunofluorescence (IF) from patients of Ninth People's Hospital, Shanghai JiaoTong University School of Medicine from 2007 to 2017. The histological features of all specimens were evaluated by pathologists according to the standard criteria, and the clinic pathological characteristics of ocular melanoma patients are listed in Additional file 2: Table S2 and Additional file 3: Table S3.

m⁶A RNA methylation assay

Total RNA was extracted from samples using an EZpress RNA Purification Kit (B0004). The change in m⁶A level relative to total mRNA was measured using the m⁶A RNA Methylation Quantification Kit (Colorimetric) (ab185912) following the manufacturer's protocol. Each sample was analyzed using 200 ng of RNA isolated from different cells.

Cell lines

The PIG1 human normal melanocyte cell line was kindly provided by the Department of Ophthalmology, Peking University Third Hospital. The human ocular melanoma cell lines, OCM1, OCM1a and OM431, were kindly supplied by Professor John F. Marshall (Tumor Biology Laboratory, Cancer Research UK Clinical Center, John Vane Science Centre, London, UK). The human conjunctival melanoma cell lines, CRMM1 and CM2005.1, were kindly supplied by Prof. Martine J. Jager (Leiden University Medical Center, Leiden, The Netherlands). The HEK293T human embryonic kidney cell line was purchased from the American Type Culture Collection

(Manassas, VA, USA). The cell lines used in this study were authenticated by STR profiling.

Cell culture

Human OCM1, OCM1a, OM431 and HEK293T cells were cultured in DMEM (GIBCO). PIG1 and CM2005.1 cells were cultured in RPMI 1640 medium (GIBCO). CRMM1 cells were cultured in Ham's F-12 K (Kaighn's) Medium (GIBCO). All mediums are supplemented with 10% certified heat-inactivated fetal bovine serum (FBS; GIBCO), penicillin (100 U/mL), and streptomycin (100 mg/mL) and cells are all cultured at 37 °C in a humidified 5% CO₂ atmosphere.

RNA isolation and quantitative real-time PCR

Total RNA was extracted from samples using the EZpress RNA Purification Kit (B0004), and cDNA was generated using the PrimeScript RT Reagent Kit (Takara). Quantitative real-time PCR using Powerup SYBR Green PCR Master Mix (Life Technologies) was performed using a real-time PCR system (Applied Biosystems).

Western blot analysis

Cells were harvested at the indicated times and rinsed three times with PBS. Cell extracts were prepared with lysis buffer and centrifuged at 13,000 *xg* for 30 min at 4 °C. Protein samples were separated by 7.5% (wt/vol) sodium dodecyl sulfate–polyacrylamide gel electrophoresis (SDS–PAGE) and transferred to polyvinylidene fluoride membranes. After blocking with 5% milk for 1 h at room temperature, the membrane was incubated with 2.5 µg/mL of antibody in 5% BSA overnight at 4 °C. The membrane was then incubated with a secondary antibody conjugated to a fluorescent tag (Invitrogen). The band signals were visualized and quantified using the Odyssey Infrared Imaging System (LI-COR, USA).

Plasmid construction

pLKO.1, pCDH and pCMV were used in our study. ShRNA sequences were generated by PCR and then cloned into the pLKO.1 vector. The *HINT2* overexpression cassette was generated by PCR and cloned into the pCDH vector and verified by DNA sequencing. The *YTHDF1* overexpression cassette was generated by PCR and cloned into the pCMV vector and verified by DNA sequencing.

Lentivirus packaging and generation of stable cell lines

Lipofectamine 3000 reagent (Invitrogen) was incubated with Opti-MEM I Reduced Serum Medium (GIBCO), and HEK293T cells were transfected with 3 mg of plasmid or 6.0 mg of the PsPax plasmid. Eight hours after transfection, the medium was replaced with 10 mL of fresh medium. The supernatant containing the viruses

was collected at 48 and 72 h, filtered through a 0.45-µm cellulose acetate filter and used immediately. Viruses carrying a given plasmid were premixed 1:1, and 50 µL of virus was added to 1 mL of serum. Twenty-four hours prior to transfection, tumor cells were seeded at 2.0×10^5 cells per well in a 6-cm dish, and the medium was replaced with virus-containing supernatant supplemented with 10 ng/mL polybrene (Sigma-Aldrich). After 48 h, the medium was replaced with fresh medium. Cells were selected by incubation with 4 mg/mL puromycin (InvivoGen) for 2 weeks and maintained in 1 mg/mL puromycin (InvivoGen).

Cell proliferation/growth assays

Cell proliferation/growth was assessed by CCK8 assays (HY-K0301, MCE) following the manufacturer's instructions. Briefly, cells were seeded in triplicate in 96-well plates at a density of 2000–10,000 cells/100 mL. Dye solution was added at the indicated time points, and the plates were incubated at 37 °C for 3–4 h before the absorbance was detected at 570 nm.

Apoptosis assays

FITC-Annexin V Apoptosis Detection Kit 1 (BD Biosciences, San Diego, CA) was used following the manufacturer's instructions. Briefly, cells were washed twice with cold PBS, stained with FITC-Annexin V and PI on ice for 5 min, and subjected to flow cytometric analysis using a BD LSRFortessa analyzer (BD Biosciences).

Colony formation assay

A volume of 1 mL of complete medium containing 1000 cells was placed in each well of a six-well plate. The plate was stained with 0.25% crystal violet after 1–2 weeks.

Transwell assay

A 24-well transwell system (Corning) with polycarbonate filters (8-µm pores, Corning) was used. The upper compartment contained 10,000 cells suspended in the appropriate medium with 2% FBS; the lower chamber contained 10% FBS. After 1 day of incubation at 37 °C, the cells in the transwell system were stained with 0.25% crystal violet. The cells remaining in the upper transwell chamber were removed, and those that migrated to the lower chamber were photographed and counted.

Cell cycle analysis

A sample of approximately 10^6 cells was centrifuged at 800 *xg* for 4 min, washed twice with PBS, resuspended in 1 mL of PBS and fixed in 75% ethanol overnight at –20 °C. The fixed cells were washed three times with 10 mL of ice-cold PBS, resuspended in 200–400 mL of PBS containing 10 mL of RNase (Qiagen) and incubated at

37 °C for 30 min in the dark. The cells were then subjected to FACS at the Flow Cytometry Facility.

RNA extraction, library construction, Illumina sequencing (RNA-seq) and data analysis

Total RNA was extracted from samples using the EZpress RNA Purification Kit (B0004). We confirmed the integrity of the RNA using the 2100 Bioanalyzer (Agilent Technologies, USA) and measured the RNA concentration using a Qubit 2.0 fluorometer with a Qubit RNA Assay Kit (Life Technologies, Carlsbad, CA, USA). We then prepared libraries from 100 ng of total RNA using the Illumina TruSeq RNA Sample Prep Kit (San Diego, CA, USA) following the manufacturer's protocol.

Methylated RNA immunoprecipitation sequencing (MeRIP-seq)

MeRIP was performed as previously described [17]. Briefly, purified mRNA was randomly fragmented to approximately 100 nucleotides using Ambion RNA fragmentation reagents and then subjected to IP with an anti-m⁶A antibody (202,003, Synaptic Systems) and protein A magnetic beads (88,845, Pierce) in MeRIP buffer (150 mM NaCl, 10 mM Tris-HCl, pH 7.4, 0.1% NP-40) supplemented with RNase inhibitor. m⁶A-containing mRNA fragments were eluted with m⁶A in MeRIP buffer and purified using TRIzol reagent. For MeRIP-seq, two sets of samples were collected for duplicate biological repeats. For MeRIP-qRT-PCR, the same procedures were followed, except that the purified mRNA was fragmented to approximately 200 nucleotides; three biological repeats were conducted. The samples were sequenced with an Illumina HiSeq 4000 platform.

Cross-linking and methylated RNA immunoprecipitation (miCLIP) -SMARTer-m⁶A-seq

Small-scale, single base-resolution m⁶A methylome detection was carried out following procedures modified from a previous report. Briefly, 100 ng of mRNA was isolated from the tumor (OCM1, OCM1a, OM431, CRMM1 and CM2005.1) and normal (PIG1) cell lines using the Dynabeads mRNA Purification Kit (Life Technologies, 61,006), fragmented to ~100 nucleotides using fragmentation reagent (Life Technologies, AM8740), and incubated with 5 µg of an anti-m⁶A antibody (Abcam, ab151230) in 450 µL of IP buffer (50 mM Tris, 100 mM NaCl, 0.05% NP-40, adjusted to pH 7.4) under gentle rotation at 4 °C for 2 h. The mixture was transferred to a clear flat-bottom 96-well plate (Corning) on ice and irradiated three times with 0.15 J/cm² at 254 nm using a CL-1000 Ultraviolet Crosslinker (UVP). After irradiation, the mixture was collected and incubated with 50 µL of pre-washed Dynabeads Protein A (Life Technologies, 1001D) at 4 °C for 2 h. After extensive washing twice with high-

salt buffer (50 mM Tris, 1 M NaCl, 1 mM EDTA, 1% NP-40, 0.1% SDS, adjusted to pH 7.4) and twice with IP buffer, the samples on the beads were subjected to dephosphorylation with T4 PNK (NEB, M0201 L) at 37 °C for 20 min. The RNA was then eluted from the beads by proteinase K (Sigma, P2308) treatment at 55 °C for 1 h, followed by phenol-chloroform extraction and ethanol precipitation. The purified RNA was subjected to library construction using the SMARTer smRNA-Seq Kit for Illumina (Clontech Laboratories, 635,030) according to the manufacturer's instructions and sequenced using the Illumina HiSeq X Ten platform.

RNA-binding protein immunoprecipitation (RIP)-qPCR

To examine m⁶A modification or RNA-binding proteins on individual genes, the Magna RIP™ Quad RNA-Binding Protein Immunoprecipitation Kit (17-704, Millipore, Billerica, MA) was used according to the manufacturer's instructions. Briefly, 200 mg of total RNA was enriched with antibody- or rabbit IgG-conjugated Protein A/G Magnetic Beads in 500 mL of 1x IP buffer supplemented with RNase inhibitors at 4 °C overnight. RNA of interest was immunoprecipitated with the beads. One-tenth of each fragmented RNA sample was saved as the input control and further analyzed by qPCR.

Sequencing data analysis

For all untreated tumor and normal cell lines, RNA-seq generated paired-end reads with a length of 151 bp, and MeRIP-seq generated single-end reads with a length of 151 bp. Cutadapt software (version 1.18) [18] was used to trim off the adapter sequences for all raw reads. Reads that contained an ambiguous nucleotide or with lengths less than 18 nt were discarded by Trimmomatic (version 0.36) [19].

The remaining reads were aligned to the human genome (version hg19) using Hisat2 (version 2.1.0) [20]. Only uniquely mapped reads with a mapping quality score ≥ 20 were kept for the subsequent analysis for each sample.

For MeRIP-seq, MACS2 software (version 2.0.10) [21] was used for m⁶A peak calling in each MeRIP sample with the corresponding input sample serving as a control. The default options expected for '-nomodel, -keep-dul all' to turn off fragment size estimation and to keep all uniquely mapped reads in MACS2 were set. Software BEDTools' intersectBed (version 2.27.1) [22] was used to annotate each peak on the Ensembl (release 72) gene annotation information.

For RNA-seq, the number of reads mapped to each Ensembl (release 72) gene was counted using the software featureCounts (version 1.6.3) [23] from Subread package. FeatureCounts was applied with default options

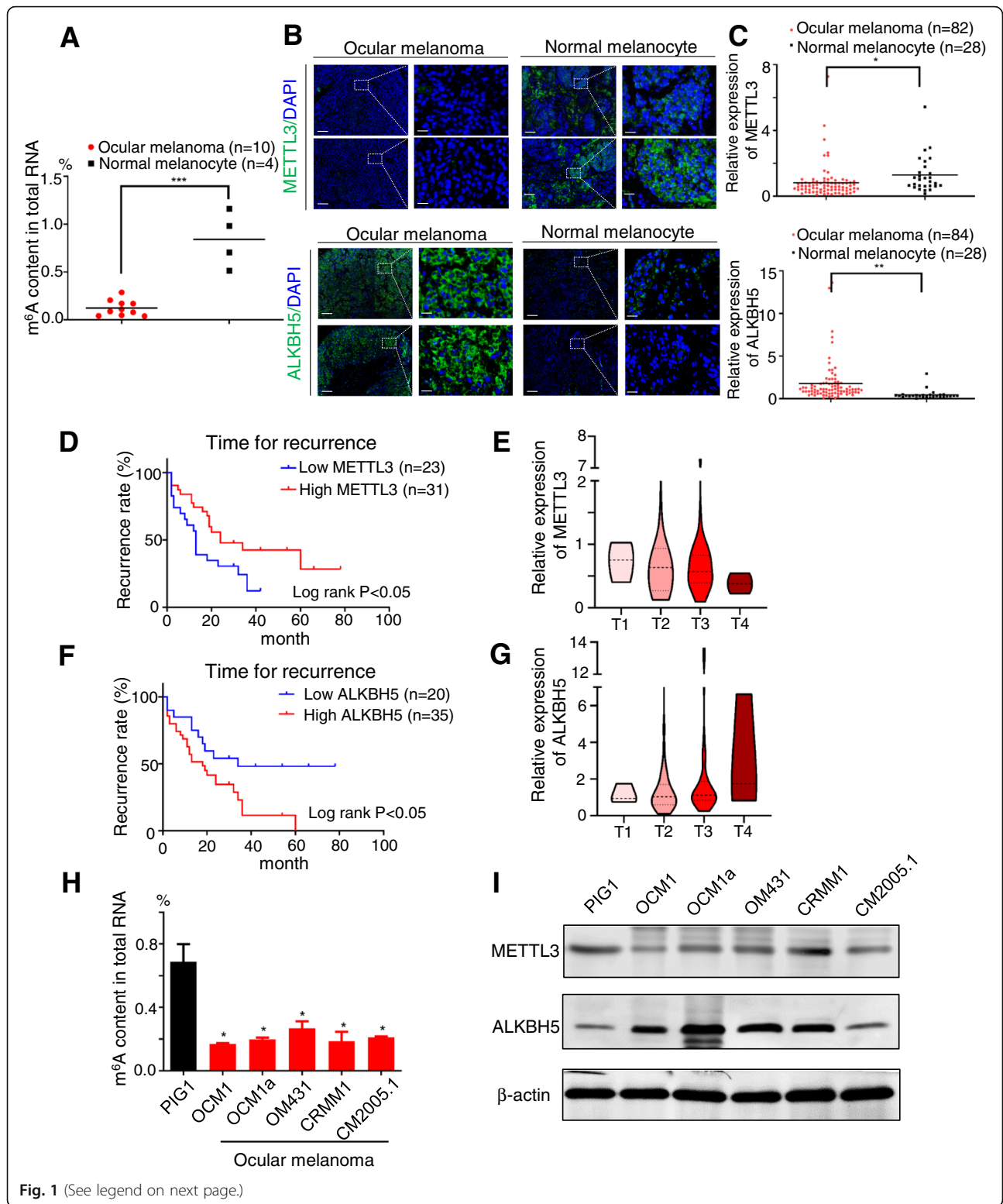


Fig. 1 (See legend on next page.)

(See figure on previous page.)

Fig. 1 Ocular melanoma exhibited decreased m⁶A levels, which was associated with poor prognosis. **a** An m⁶A RNA methylation assay revealed the m⁶A content in tumor and adjacent normal tissues. For ocular melanoma, $n = 10$, for normal melanocyte, $n = 4$, $***p < 0.001$. **b, c** METTL3 and ALKBH5 expression in normal and tumor tissues. **B:** METTL3 and ALKBH5 expression according to IF analysis. Scale bar: left panel, 100 μm ; right panel, 20 μm . **C:** Statistical results of METTL3 and ALKBH5 expression in normal and tumor tissues. $*p < 0.05$, $***p < 0.001$. **d** Kaplan-Meier curves of tumor recurrence showing the difference between ocular melanoma patients with low and high METTL3 levels. $n = 54$, log rank test, $p < 0.05$. **e** The expression of METTL3 in patients at AJCC stages T1 to T4. **f** Kaplan-Meier curves of tumor recurrence showing the difference between ocular melanoma patients with low and high ALKBH5 levels. $n = 55$, log rank test, $p < 0.05$. **g** The expression of ALKBH5 in patients at AJCC stages T1 to T4. **h** The m⁶A RNA methylation assay revealed the m⁶A content in PIG1 cells and ocular melanoma cells. Error bars indicate the mean \pm SEM, $n = 3$, $*p < 0.05$. **i** Western blot showing METTL3 and ALKBH5 expression in normal melanocytes and orbital melanoma cells. The METTL3 signal was quantified and normalized to that of β -actin

expect for '-s 2, -p' to inform strand-specific library construction and fragment counting for paired-end reads.

Statistical analysis of differentially expressed genes and genes with differential protein levels

Differentially expressed genes between normal (PIG1) and tumor (OCM1, OCM1a, OM431, CRMM1 and CM2005.1) cell lines were determined using the R-package DESeq2 [24]. Transcripts with a fold change cutoff > 1.5 or < -1.5 and a p -value cutoff < 0.05 were considered significantly differentially expressed genes. Genes with differential protein levels were also determined with the same cutoffs as above.

Gene ontology analysis

Gene Ontology (GO) analysis of specific genes was performed using DAVID (<http://david.abcc.ncifcrf.gov/>). GO terms with $P < 0.05$ were statistically significant. Enrichment maps (Fig. 3e, Fig. 4b) were constructed using Cytoscape 3.7.0 installed with the Enrichment Map plugin. Within the enrichment maps, each node represents a GO pathway, and the node size is proportional to the total number of genes in each pathway. The edge thickness represents the number of overlapping genes between nodes. GO pathways of similar functions are sorted into one group, marked with labels and cycles. The number of genes in each cluster is labeled [3].

Analysis of miCLIP sequencing data

As previously reported [25], raw read preprocessing was performed. Fastx_clipper from fastx_toolkit (http://hanonlab.cshl.edu/fastx_toolkit) was used to trim off the adapter sequence of the raw reads. Fastq_filter.pl, a Perl script from the CLIP Tool Kit (CTK) [26] was used to filter out the low-quality bases, and reads with lengths shorter than 18 nt were discarded. We processed the paired-end data according to the previously reported approach [25] with the same criteria. For individual replicates, we demultiplexed the forward reads based on 5' barcodes by performing fastq2 collapse to remove PCR-amplified reads, and we reverse complemented the reverse reads and processed them in the same way as the

forward counterparts. Finally, stripBarcode.pl was performed to strip the random barcodes of the remaining reads and move to read headers for subsequent analysis processed by the CIMS pipeline.

BWA software (version 0.7.10) [27] was used to map the remaining reads to the human genome (version hg19), and an error rate (substitutions, insertions, or deletions) of ≤ 0.06 per read was allowed by setting parameter 'bwa aln -n 0.06 -q20', following the CTK Online Documentation (https://zhanglab.c2b2.columbia.edu/index.php/CTK_Documentation). The mode of mutation calling was performed as previously reported with minor modifications [28] to identify the m⁶A locus. Program CIMS.pl [29] was used to determine the coverage of the tag number (k) and mutations (m) for each mutation position. The mutation position with $m > 1$, $m/k \geq 0.01$ and $m/k \leq 0.5$ were kept, and only mutation positions within the RRACH motif were determined as m⁶A for the subsequent analysis to remove the potential m⁶Am modification [28, 30].

Motif identification within m⁶A peaks

m⁶A peaks were identified by extending 25 nt both downstream and upstream of the m⁶A sites. The motifs enriched in m⁶A peaks were analyzed by HOMER (version 4.10.3) [31]. Motif length was restricted to 5 nucleotides. The nearby peaks were merged to one peak by performing BEDTools' merge (version 2.27.1) [22]. These peaks were used as target sequences, and background sequences were constructed by randomly shuffling peaks onto total mRNAs in the genome using BEDTools' shuffleBed (version 2.27.1) [22].

Immunofluorescence (IF)

Cells adhering to a glass slide were fixed with 4% formaldehyde (Fisher) for 15 min and then blocked with 5% normal goat serum (Vector) with or without 0.1% Triton X-100 in PBS for 60 min at room temperature. Immunostaining was performed using the appropriate primary and secondary antibodies. Nuclei and the cytoskeleton were counterstained with DAPI and phalloidin, respectively. IF staining was performed with the appropriate

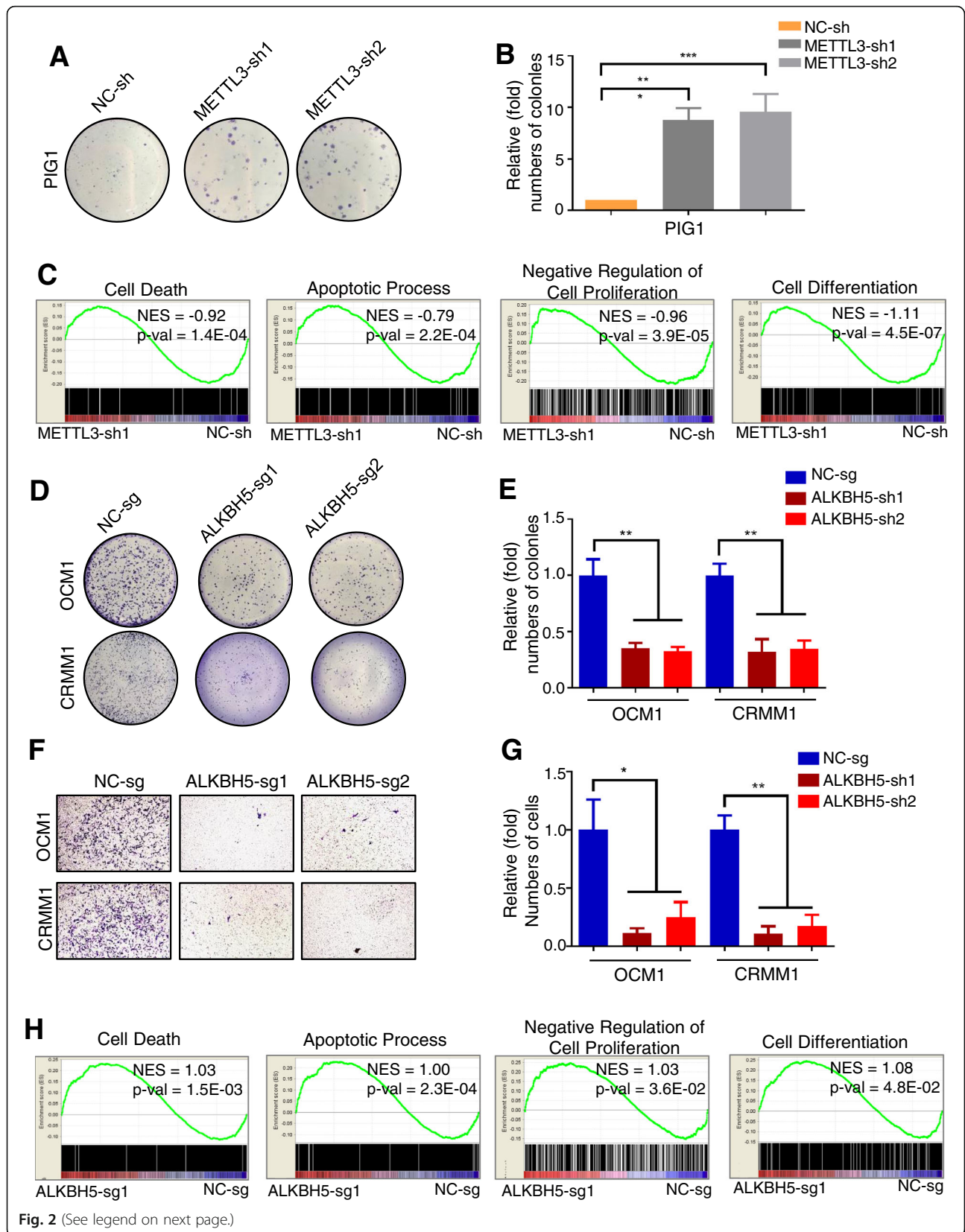


Fig. 2 (See legend on next page.)

(See figure on previous page.)

Fig. 2 m⁶A methylation inhibited ocular melanoma tumorigenesis. **a** A colony formation assay was performed to assess the tumor growth of PIG1 cells with or without *METTL3* knockdown. **b** Statistics of visible colonies in colony formation assays performed using PIG1 cells with or without *METTL3* knockdown. The colony number of the control group was set to 1. All of the experiments were performed in triplicate, and relative colony formation rates are shown as the mean ± SEM. $n = 3$, *** $p < 0.001$. **c** GSEA plots evaluating the changes in apoptosis, cell differentiation and cell death in normal melanocyte cells with or without *METTL3* knockdown. NES, normalized enrichment score. **d** A colony formation assay was performed to assess the tumor growth of ocular melanoma cells with or without *ALKBH5* knockdown. **e** Statistics of visible colonies in colony formation assays performed using ocular melanoma cells with or without *ALKBH5* knockdown. The colony number of the control group was set to 1. All of the experiments were performed in triplicate, and relative colony formation rates are shown as the mean ± SEM. $n = 3$, ** $p < 0.01$. **f** A transwell assay was performed to evaluate the migratory ability of ocular melanoma cells with or without *ALKBH5* knockdown. **g** Statistics of cells in the transwell assay performed using ocular melanoma cells with or without *ALKBH5* knockdown. The value obtained for the control group was set to 1. All of the experiments were performed in triplicate, and relative metastasis rates are shown as the mean ± SEM. $n = 3$, * $p < 0.05$, ** $p < 0.01$. **h** GSEA plots evaluating the changes in apoptosis, cell differentiation and cell death in ocular melanoma cells with or without *ALKBH5* knockdown. NES, normalized enrichment score

Alexa Fluor 488 or Alexa Fluor 546 secondary antibody (Invitrogen, 1:1000 dilution). Images were taken with a ZEISS Axio Scope A1 Upright Microscope.

RNA pull-down

Biotin-labeled ssRNA probes were synthesized in vitro by Sangon Biotin (Shanghai) Co., Ltd. In vitro RNA-protein pull-down assay were performed using Pierce™ Magnetic RNA-Protein Pull-Down Kit (Thermo Scientific, 20,164) according to the manufacturer's instructions. The cell lysate was prepared using standard lysis buffers (Thermo Scientific Pierce IP Lysis Buffer) as suggested. 100 pmol of RNA and 50 μL of magnetic beads were used per sample. Input RNA of each sample was mixed with 1 μL 50% glycerol, separated on the 8% native 1x TBE gel, and visualized by phosphorimaging using the Personal Molecular Imager (Bio-Rad) [32–37].

Luciferase reporter assay

Cells seeded in 6-well plates were transfected with the psiCHECK.2-based luciferase vector fused or not fused to the wild-type or mutated HINT2–3'UTR. Transfection efficiency was quantified by cotransfection with an actin promoter-driven Renilla luciferase reporter. The activities of firefly and Renilla luciferase in each well were calculated using a dual luciferase reporter assay system (Promega). The relative luciferase activity of the HINT2–3'UTR plasmid was further normalized to the signal in cells transfected with the firefly luciferase vector control under the same treatment conditions.

Polysome profiling

We followed previously reported protocols (<https://www.jove.com/pdf/51455/jove-protocol-51455-polysome-fractionation-analysis-mammalian-translatomes-on-genome-wide>) with the following modifications. Before collection, 0.1 mg/mL cycloheximide (CHX)

was added to the culture medium for 5 min. A sample of 150 million cells from each group was harvested, rinsed in cold PBS with 0.1 mg/mL CHX and quickly frozen in liquid nitrogen before lysis. The lysis buffer was formulated as 10 mM Tris-HCl (pH 7.5), 100 mM NaCl, 30 mM MgCl₂, and 0.1 mg/mL CHX with freshly added 1:100 protease inhibitor (Roche) and 40 U/mL SUPERase in RNase Inhibitor (Ambion). The sample was homogenized using a liquid nitrogen grinder. We chose a linear 10 to 40% sucrose gradient according to cell type, and the sample was fractionated into 23 fractions (0.5 mL per fraction) and analyzed using a Gradient Station (BioCamp) equipped with an ECONOUV monitor (BioRad, Hercules, CA) and a Gilson FC203B fraction collector (Mandel Scientific, Guelph, Canada). RNA was purified from fractions 5–22 and subjected to qPCR analysis.

Mice and animal housing

The animal experiments were approved by the Shanghai Jiao Tong University Animal Care and Use Committee and conducted in accordance with the animal policies of Shanghai JiaoTong University and the guidelines established by the National Health and Family Planning Commission of China. Cells were harvested by trypsinization and washed twice with PBS (GIBCO). BALB/c nude mice (male, 6 weeks old) were used for the study.

Tumorigenesis assay in vivo

Approximately 1×10^6 melanoma cells from each group were injected subcutaneously into the right side of the abdomen of BALB/c nude mice (male, 6 weeks old). At 30 days after cell injection, the mice were humanely killed, and the tumors were harvested. Each tumor was fixed in 4% formaldehyde, embedded in paraffin, and examined for tumor formation by histologic analysis of hematoxylin and eosin (H&E)-stained sections. Tumor volume was calculated by the

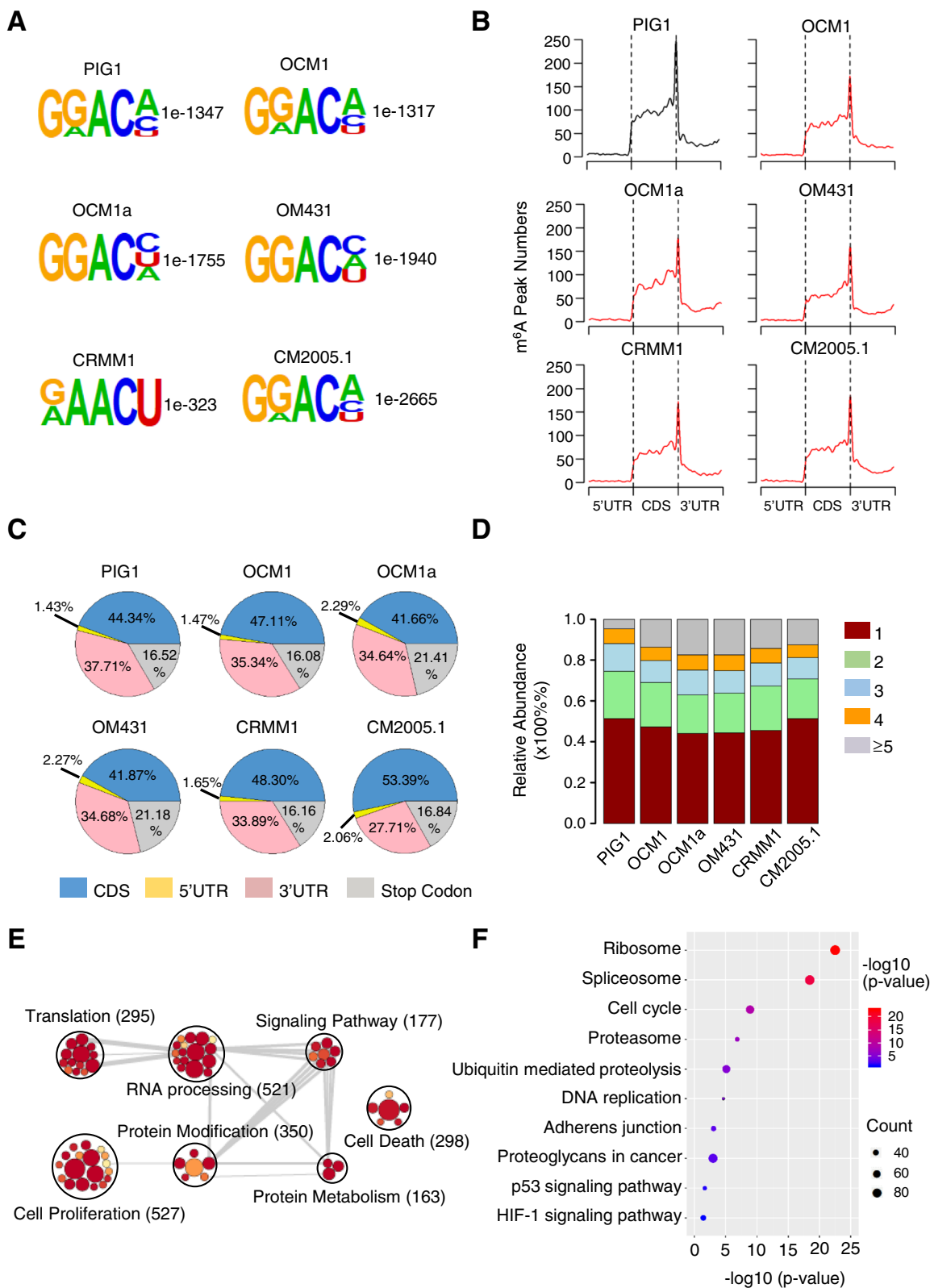


Fig. 3 (See legend on next page.)

(See figure on previous page.)

Fig. 3 Dynamic m⁶A modifications were highly associated with ocular melanoma tumorigenesis. **a** Top enriched motifs within m⁶A peaks identified in ocular melanoma and normal cells. **b** Distribution of m⁶A sites along the length of mRNA transcripts. **c** Pie charts showing the m⁶A peak distribution in different RNA regions (CDS, 5' UTR, 3' UTR and stop codon) in ocular melanoma and normal cells. **d** The percentage of methylated genes with 1, 2, 3, 4 or more than 5 peaks per gene in each cell line. **e** GO enrichment map of m⁶A-containing genes in ocular melanoma and normal cells. **f** KEGG pathway analysis of m⁶A-modified genes in ocular melanoma and normal cells

formula $V = ab^2/2$, where a and b are tumor length and width, respectively.

Immunohistochemistry (IHC)

Tissue slides were deparaffinized and rehydrated through an alcohol series, followed by antigen retrieval with sodium citrate buffer. Tumor sections were blocked with 5% normal goat serum (Vector) with 0.1% Triton X-100 and 3% H₂O₂ in PBS for 60 min at room temperature and then incubated with appropriate primary antibodies at 4 °C overnight. IHC was performed with horseradish peroxidase (HRP) conjugates using DAB detection.

Results

Decreased m⁶A in ocular melanoma

To study the functional role of m⁶A methylation in malignant ocular melanoma, we first examined the global m⁶A level in ocular melanoma relative to normal control samples. A significant decrease in m⁶A modification in cellular mRNAs was observed in tumor samples ($p < 0.001$) (Fig. 1a; Additional file 1: Table S1). Notably, the expression of the known m⁶A “writer” METTL3 was also decreased in ocular melanoma tissue compared to normal melanocyte tissue ($p < 0.05$) (Fig. 1b; Additional file 2: Table S2; Additional file 3: Table S3), while the opposite trend was observed for m⁶A “eraser” ALKBH5 ($p < 0.01$) (Fig. 1c; Additional file 2: Table S2; Additional file 3: Table S3). Thus, the decreased m⁶A level in ocular melanoma cells (Fig. 1a) is likely due to the downregulation of METTL3 and upregulation of ALKBH5. Furthermore, lower expression of METTL3 predicted earlier recurrence and enhanced aggressiveness (log rank test, $p < 0.05$) (Fig. 1d, e, Additional file 2: Table S2; Additional file 3: Table S3). Similarly, elevated ALKBH5 expression indicated a poor prognosis (log rank test, $p < 0.05$) (Fig. 1f, g, Additional file 2: Table S2; Additional file 3: Table S3), suggesting that a reduced global m⁶A level predicts higher malignancy. Consistently, we also observed decreased m⁶A modification in ocular melanoma cells (Fig. 1h). Accordingly, decreased METTL3 and upregulated ALKBH5 were observed in ocular melanoma cells (Fig. 1i). These data indicate that a large portion of ocular melanoma is characterized by decreased m⁶A

modification, either through decreased METTL3 expression or increased ALKBH5 expression.

m⁶A methylation inhibits ocular melanoma

To evaluate whether the global m⁶A level is related to tumorigenesis in ocular melanoma, we first inhibited the expression of methyltransferase *METTL3* in normal pigmented cells and ocular melanoma cells. The *METTL3* expression level decreased to ~30% of the original level in normal control cells, PIG1 (Additional file 4: Figure S1A-B), and the global m⁶A level decreased when *METTL3* was knocked down (Additional file 4: Figure S1C), as expected. After silencing *METTL3*, normal melanocyte cells formed an enlarged colony (Fig. 2a, b) with increased growth (Additional file 4: Figure S1D), reduced apoptosis (Additional file 4: Figure S1E), and an increased population in S phase, indicating faster cell division (Additional file 4: Figure S1F). Furthermore, genome-wide gene set enrichment analysis (GSEA) indicated that lower global m⁶A methylation promotes tumorigenesis and identified major regulations of *METTL3* (Fig. 2c). Similarly, we silenced the expression of methyltransferase *METTL3* in ocular melanoma. OCM1 and CRMM1 cells were transfected with the same *METTL3* shRNA, and *METTL3* expression levels were successfully knocked down to ~20% of the original levels (Additional file 5: Figure S2A-B). Next, we evaluated changes in proliferation and tumorigenesis and found that the colony formation rate increased to almost 200% in melanoma cells with lower m⁶A methylation (Additional file 5: Figure S2C-D). Melanoma cells with *METTL3* knockdown also displayed significantly greater migratory ability (Additional file 5: Figure S2E-F) and slightly accelerated cell growth (Additional file 5: Figure S2G-H).

Because tumor cells present decreased m⁶A modifications, we next inhibited the expression of the demethylase *ALKBH5*. CRISPR/Cas9 is utilized to delete *ALKBH5* in OCM1 and CRMM1 cells (Additional file 6: Figure S3A), and m⁶A methylation increases significantly when *ALKBH5* is knocked down (Additional file 6: Figure S3B). Moreover, the rate of colony formation decreased to 20% in melanoma cells with higher m⁶A methylation (Fig. 2d, e), and these cells showed a significantly weaker migratory ability (Fig. 2f, g).

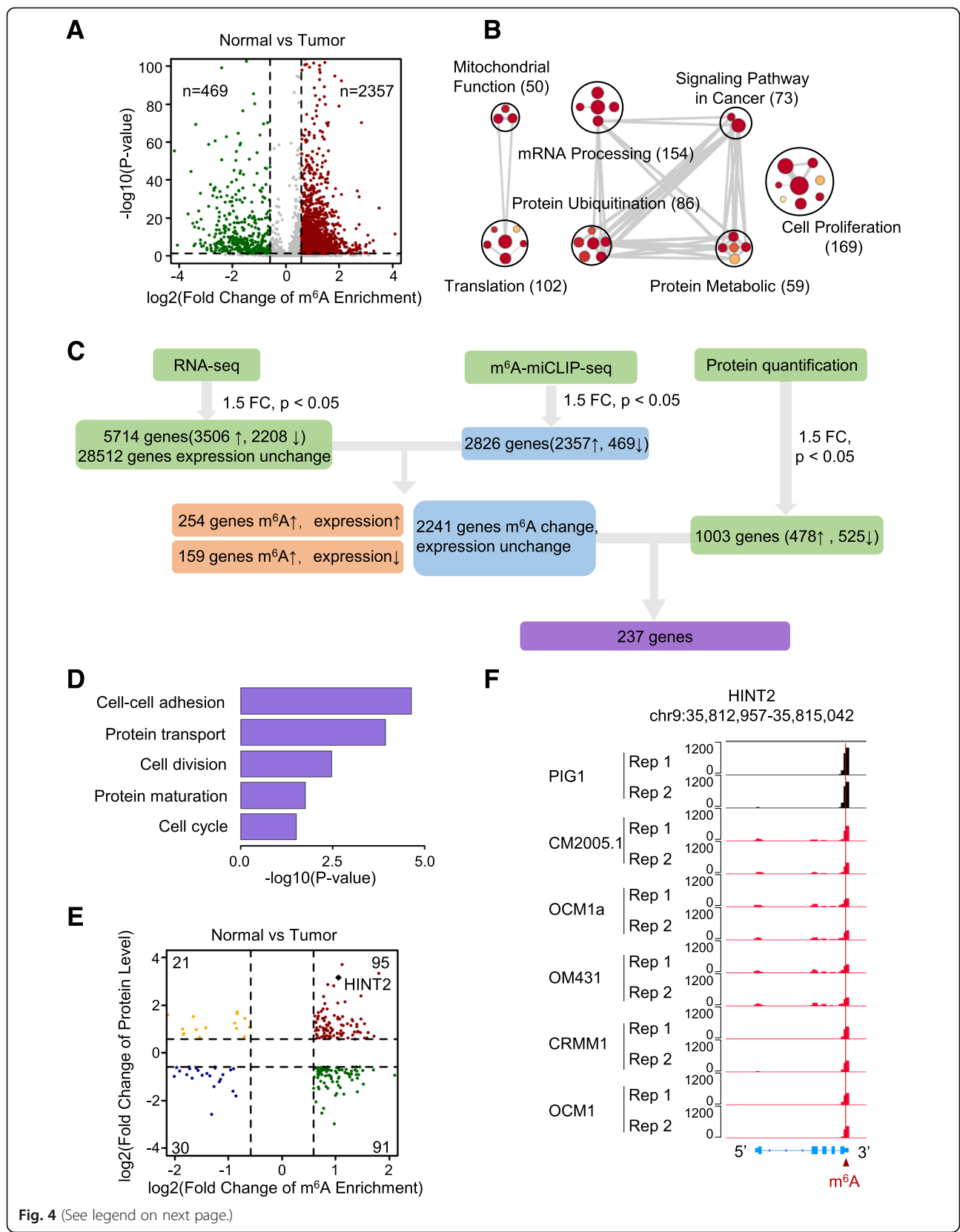


Fig. 4 (See legend on next page.)

(See figure on previous page.)

Fig. 4 Transcriptome-wide identification of m⁶A targets that regulate tumorigenesis. **a** Volcano plots showing m⁶A enrichment of genes in normal and tumor cells. **b** GO enrichment map of genes with specific enriched m⁶A peaks in control normal cells. **c** Schematic of m⁶A modification downstream analysis. In normal cells, RNA-seq detected 5714 genes with differential expression in which 3506 genes were upregulated and 2208 genes were downregulated. m⁶A-miCLIP-seq showed that 2826 genes were differentially methylated. In normal cells, 2357 genes were up-methylated, and 469 genes were down-methylated. Protein quantification analysis revealed 1003 genes with differential protein levels in normal cells: 478 genes had upregulated protein levels, and 525 genes had downregulated protein levels. In the group of genes with higher m⁶A levels, 254 genes were upregulated, and 159 genes were downregulated. However, 2241 genes with m⁶A methylation levels showed no expression change in normal cells. Finally, we found that 237 genes also had differential m⁶A levels with differential protein levels. The cutoffs used for differentially expressed genes, differential methylation levels and genes with differential protein levels were $FC < -1.5$ or $FC > 1.5$ and $p < 0.05$. FC: fold change, p : p -value. **d** Representative GO biological process categories enriched in genes with significant differences in m⁶A enrichment and protein content but not gene expression. **e** Volcano plots showing the m⁶A enrichment and protein content of genes in normal cells compared to tumor cells. **f** IGV tracks displaying the miCLIP-seq reads coverage of *HINT2* in normal and tumor cells

Compared with control cells, ocular melanoma cells with higher m⁶A methylation exhibited significantly decreased tumor growth (Additional file 6: Figure S3C) as more cells underwent apoptosis (Additional file 6: Figure S3D) and fewer cells underwent cell division (Additional file 6: Figure S3E). Genome-wide RNA-seq and GSEA of ocular melanoma cells further demonstrated these antitumor effects of higher m⁶A modification levels and identified major target gene clusters of *ALKBH5* (Fig. 2h).

Transcriptome-wide m⁶A-Seq and RNA-seq assays to identify potential m⁶A-mediated targets

To understand the regulatory role of m⁶A modification in gene expression, we mapped the m⁶A sites of normal and ocular melanoma cells by MeRIP-seq and m⁶A individual-nucleotide-resolution cross-linking and immunoprecipitation with sequencing (miCLIP-seq), with two independent biological replicates (Additional file 7: Figure S4A). An average of 13,083 and 11,750 m⁶A peaks were identified from miCLIP-seq libraries generated from normal and tumor cells (Additional file 7: Figure S4B). Consistent with previous m⁶A-seq results [3, 4], the m⁶A peaks we identified were characterized by the canonical RRACH motif (Fig. 3a; Additional file 7: Figure S4C) and were enriched in the 3' UTR, especially near the stop codons (Fig. 3b, c; Additional file 7: Figure S4D-F). Although the motif and the pattern of m⁶A distribution were observed similarly in all cells, we found that the m⁶A modifications were reduced globally in tumor cells compared to normal control cells (Additional file 7: Figure S4G) and that there were more genes with only one m⁶A site in normal cells among the detected m⁶A peaks (Fig. 3d). In total, we identified 5828 genes with significant m⁶A modifications (Additional file 7: Figure S4E). In these genes, terms of cell proliferation and cell death were significantly enriched (Fig. 3e). Moreover, HIF-1 and p53 signaling pathway were significantly enriched to be regulated (Fig. 3f), suggesting a regulation role of m⁶A modification in tumorigenesis.

In detail, the number of transcripts with greater enriched m⁶A modifications in normal cells was more than 5 times higher than that in tumor cells (Fig. 4a). These transcripts participate in several signaling pathways related to cell proliferation and tumorigenesis (Fig. 4b, Additional file 8: Figure S5A).

To systematically illuminate gene expression changes resulting from the decreased m⁶A modification in ocular melanoma, we used RNA sequencing to compare the transcriptome between normal and tumor cells. Since m⁶A modifications play a key role in the modulation of translation [2], we associatively analyzed the protein expression of genes and, as expected, many genes with m⁶A modifications were inconsistent between mRNA expression and protein expression (Fig. 4c, third panel; Additional file 12: Table S4), suggesting a potential post-transcriptional modulation of translation of m⁶A modifications. Consistently, these genes are involved in the cell cycle, cell adhesion and protein processes (Fig. 4d). *HINT2*, one of the genes with most significant evaluated protein expression and m⁶A enrichment in normal cells, was chosen as a typical example for analyzing the mechanism of m⁶A modifications acting as translation modulators in tumorigenesis (Fig. 4e, Additional file 8: Figure S5C). From our miCLIP-seq data, we identified a statistically significant m⁶A peak in *HINT2* mRNA on the 3'UTR, which was especially enriched in normal cells (Fig. 4f). To confirm our results, we verified decreased m⁶A modifications of *HINT2* mRNA, downregulated expression of *HINT2* protein, and unnoticeably altered mRNA levels by RNA-binding protein immunoprecipitation (RIP)-qPCR, Western blotting and qPCR (Additional file 10: Figure S6A-C).

HINT2 suppresses ocular melanoma in an m⁶A-dependent manner

HINT2 has been reported to act as a tumor suppressor in hepatocellular carcinoma and pancreatic cancer [38, 39], and we confirmed its function in ocular melanoma.

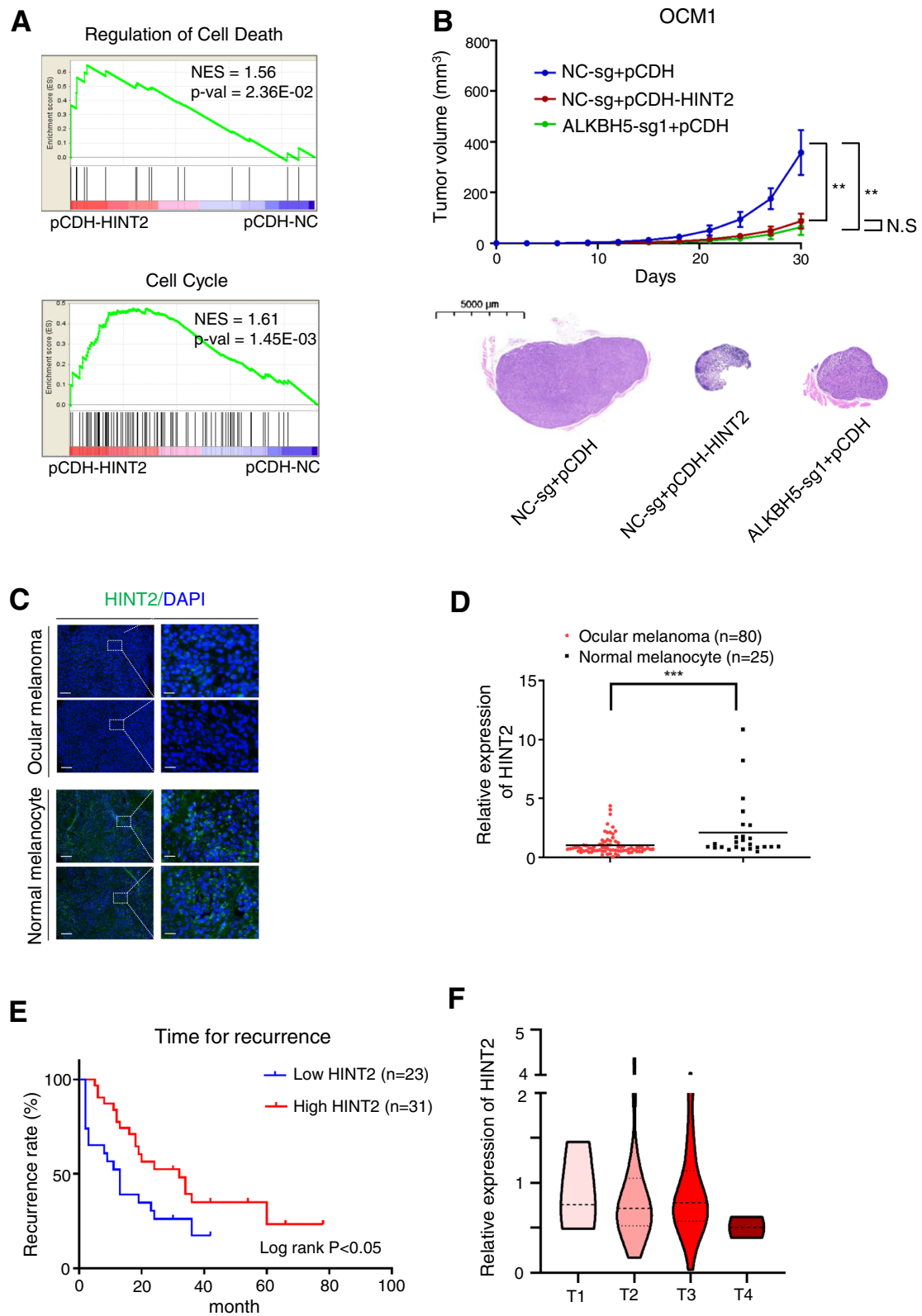


Fig. 5 (See legend on next page.)

(See figure on previous page.)

Fig. 5 *HINT2* acted as a tumor suppressor gene in ocular melanoma cells. **a** GSEA plots evaluating the changes in autophagy, mitochondrial function, apoptosis and cell death in ocular melanoma cells with or without *HINT2* overexpression. NES, normalized enrichment score. **b** The animal experiment shows tumor suppressor roles of *ALKBH5* and *HINT2* in vivo. Top: The line graph shows the volume of subcutaneous tumors formed by the indicated OCM1 cells. Bottom: representative images of H&E staining to evaluate tumor formation. $n = 5$, $**p < 0.01$; scale bar: 5 mm. **c, d** *HINT2* expression in normal and tumor tissues. C: *HINT2* expression according to IF analysis. Scale bar: top panel, 100 μm ; bottom panel, 20 μm . D: Statistical results of *HINT2* expression in normal and tumor tissues. $n = 105$, $***p < 0.001$. **e** Kaplan-Meier curves of tumor recurrence showing the difference between ocular melanoma patients with low and high *HINT2* levels. $n = 54$, log rank test, $p < 0.05$. **f** The expression of *HINT2* in patients at AJCC stages T1 to T4

We overexpressed *HINT2* in ocular melanoma cells at both the mRNA (Additional file 10: Figure S6D) and protein (Additional file 10: Figure S6E) levels. Notably, cell proliferation (Additional file 10: Figure S6F), cell migration (Additional file 10: Figure S6G-H) and colony formation (Additional file 10: Figure S6I-J) were significantly inhibited and apoptosis was increased (Additional file 10: Figure S6K) in ocular melanoma cells upon *HINT2* overexpression. In addition, GSEA showed that *HINT2* promoted apoptosis and cell death in tumor cells (Fig. 5a). To determine the role of *HINT2* in tumor characteristics in vivo, we performed subcutaneous transplantation of ocular melanoma cells with different treatments. We thus tested the tumor suppression role of *HINT2* by overexpressing *HINT2*. In the *HINT2*-overexpressing group (Fig. 5b, Group B) compared with the empty vector group (Fig. 5b, Group A), we found that tumor volume was persistently reduced ($p < 0.01$), meeting the changes created by increased global m⁶A modification (Fig. 5b, Group C). To investigate whether these variations in protein expression occur in samples, we performed IF staining in ocular melanoma and normal tissue and found that *HINT2* was indeed downregulated in tumor samples ($p < 0.001$) (Fig. 5c, d). Notably, lower *HINT2* expression in ocular melanoma tissue samples was highly correlated with a poor prognosis (log rank test, $p < 0.05$) (Fig. 5e, f; Additional file 2: Table S2; Additional file 3: Table S3).

Because *HINT2* restrains cell growth and migration in ocular melanoma and shows reduced m⁶A methylation in tumors compared to normal cells, we hypothesized that decreased m⁶A modification might restrain tumor growth partially through upregulating *HINT2* expression. The m⁶A status of *HINT2* mRNA was further measured by MeRIP of fragmented RNA, and the m⁶A peak on the 3'UTR was specifically methylated by METTL3 and demethylated by ALKBH5, suggesting functional relevance (Fig. 6a, b). In addition, *HINT2* protein expression (Fig. 6c, d, Left), rather than mRNA expression (Fig. 6c, d, Right; Additional file 11 Figure S7A), was decreased when *METTL3* was knocked down, while it was upregulated when *ALKBH5* was knocked down, indicating that *HINT2* translation is positively regulated by its

m⁶A modifications. To determine if reduced *HINT2* expression underlies the decreased proliferation observed upon enhancing m⁶A modification in ocular melanoma, we attempted to rescue this phenotype by inhibiting *HINT2* expression in upregulated m⁶A cells (Fig. 6e, lanes 3,4). *HINT2* knockdown in *ALKBH5* knockdown cells promoted cell proliferation (Fig. 6f, lanes 3, 4, 6G-H). Importantly, the cell proliferation rates of *ALKBH5* knockdown cells after *HINT2* knockdown were only partially comparable to those of the control cells with normal *ALKBH5* expression (Fig. 6f, lanes 1,4, 6G-H), suggesting that there are more tumor-related genes regulated by their m⁶A modifications. Collectively, m⁶A-guided tumor inhibition partially results from the posttranscriptional regulation of *HINT2*.

m⁶A modification promotes *HINT2* translation

Because m⁶A methylation appears to promote the translation of *HINT2*, we hypothesized that *HINT2* transcripts are targets of the YTH family, the m⁶A reader that regulates translation of m⁶A modified transcripts [40]. RIP-qPCR analysis revealed that *HINT2* mRNAs interacted with YTHDF1 more strongly than the others (Fig. 7a). In addition, RNA pull-down assays further confirmed that YTHDF1 interacted with *HINT2* mRNA and that the m⁶A modification of *HINT2* greatly facilitated its binding to YTHDF1 (Fig. 7b, c, Additional file 15: Table S5). Consistently, *YTHDF1* knockdown (Fig. 7d line 1, Additional file 11: Figure S7B) decreased *HINT2* protein expression (Fig. 7d line 2), while *YTHDF1* overexpression (Fig. 7e, f line 1, Additional file 11: Figure S7C-D) increased *HINT2* protein expression (Fig. 7e-f line2). These changes in *HINT2* expression are not due to changes in the abundance of the *HINT2* transcript (Fig. 7d-f, Bottom); rather, the regulation of mRNA translation relies on the methylation of transcripts. We created reporter constructs with *HINT2* 3' UTR (WT) or m⁶A locus mutated (MT) sequences (Additional file 15: Table S5), and dual luciferase assays showed that *ALKBH5* significantly decreased the luciferase activity of reporters carrying the wild-type

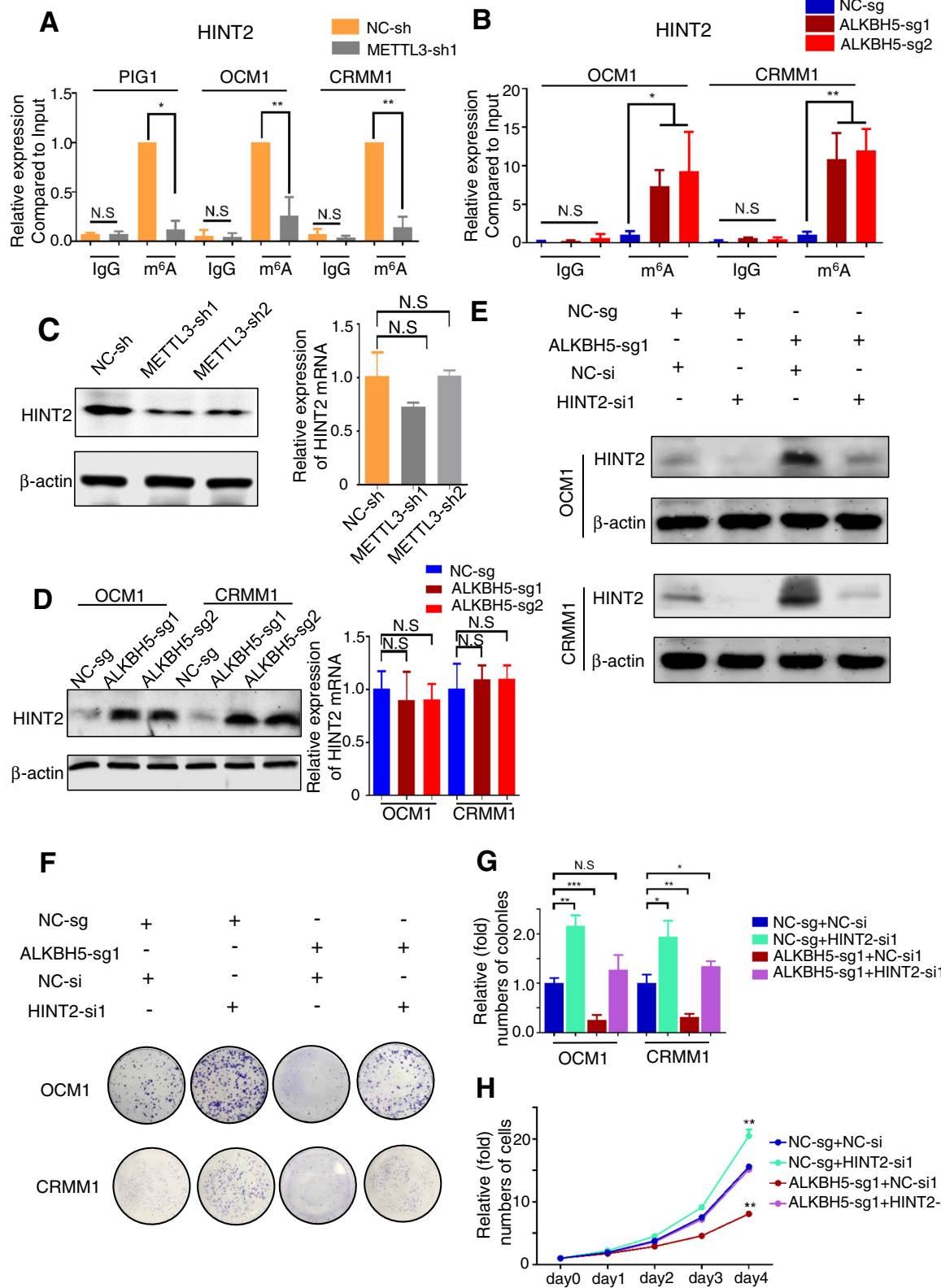


Fig. 6 (See legend on next page.)

(See figure on previous page.)

Fig. 6 HINT2 protein expression was regulated by m⁶A modification. **a** Reduction in m⁶A modification in specific regions of *HINT2* transcripts upon *METTL3* knockdown, as assessed by gene-specific m⁶A-RIP-qPCR assays, in PIG1, OCM1 and CRMM1 cells. The value obtained for the control group was set to 1. Error bars indicate the mean ± SEM, *n* = 3, **p* < 0.05, ***p* < 0.01. **b** Reduction in m⁶A modification in specific regions of *HINT2* transcripts upon *ALKBH5* knockdown, as assessed by gene-specific m⁶A-RIP-qPCR assays, in OCM1 and CRMM1 cells. The value obtained for the control group was set to 1. Error bars indicate the mean ± SEM, *n* = 3, **p* < 0.05, ***p* < 0.01. **c, d** Western blot (Left) and real-time PCR (Right) showing *HINT2* expression in PIG1 cells with or without *METTL3* knockdown (**c**) and in OCM1 and CRMM1 cells with or without *ALKBH5* knockdown (**d**). The *HINT2* signal was quantified and normalized to that of *β-actin*. Error bars indicate the mean ± SEM, *n* = 3. **e** *HINT2* expression in OCM1 and CRMM1 cells with or without *ALKBH5* knockdown and with or without *HINT2* knockdown. **f** A colony formation assay was performed to assess the tumor growth of OCM1 and CRMM1 cells with or without *ALKBH5* knockdown and with or without *HINT2* knockdown. **g** Statistical analysis of the colony formation assay performed using OCM1 and CRMM1 cells with or without *ALKBH5* knockdown and with or without *HINT2* knockdown. The colony number in the control group was set to 1. All of the experiments were performed in triplicate, and relative colony formation rates are shown as the mean ± SEM. *n* = 3, ***p* < 0.01, ****p* < 0.001. **h** Proliferation of OCM1 and CRMM1 cells with or without *ALKBH5* knockdown and with or without *HINT2* knockdown, as determined by CCK8 assays. *n* = 3, ***p* < 0.01

fragment instead of the corresponding mutant fragment (Fig. 7g). In detail, the association of the *HINT2* transcript with actively transcribing ribosomes was improved by its m⁶A modifications (Fig. 7h, Additional file 11: Figure S7E). Altogether, these experiments reveal that m⁶A modification has an impact on the translation of *HINT2* when recognized by YTHDF1.

Discussion

Here, we discovered that m⁶A mRNA methylation regulates the translation of the tumor suppressor gene *HINT2* and thereby regulates ocular melanoma tumorigenesis (Fig. 7i). One-third of mRNAs are m⁶A modified, which may regulate mRNA stability and translation [2]. A previous study discovered that the “writers” of m⁶A methylation, *METTL3* and *METTL14*, could play both oncogenic and tumor suppressor roles in numerous cancers [40, 41], while oncogenic roles have been reported for “erasers” such as *FTO* and *ALKBH5* [7, 42, 43]. Here, we found that the decreased global m⁶A modification in ocular melanoma promoted tumorigenesis, which resulted from decreased “writers” and upregulated “erasers”. Our study indicates that the disturbance of global m⁶A homeostasis is a key driver in the regulation of tumor formation, which depends on the balance of “writers” and “erasers” of m⁶A modification.

Notably, the balance of “writers” and “erasers” regulates clusters of gene function, and the AKT pathway is one of the most important targets regulated by m⁶A modifications. The expression of some key genes of the AKT pathway, such as *PHLPP2*, *PTEN*, *Bcl2* and *c-Myc*, has been reported to be regulated by their m⁶A modifications. These modifications can be written by *METTL3* or *METTL14* and can be erased by *ALKBH5* and regulate the tumorigenesis of leukemia, pancreatic cancer, endometrial cancer and gastric cancer [10, 30, 44–46]. Although we did not find a

significant regulation of the AKT pathway by m⁶A modifications in ocular melanoma, genes in other biological processes, such as mRNA processing, translation, Hippo-YAP signaling and MAPK signaling, were differentially expressed (Fig. 4b, Additional file 8: Figure S5A-C). These signaling pathways have been reported to be involved in m⁶A targets in colorectal cancer and lung cancer and in the inflammatory response [47–49]. Other tumor-related genes, such as *ACAT2*, *PIR* and *CTBP1*, were potentially regulated by m⁶A modifications in ocular melanoma. Further studies should be performed to understand m⁶A modification systematically.

Notably, the regulation mechanisms of m⁶A modifications are complicated, reflected not only in multitudinous targets but also in different regulations in various cells. It should be noted that the key enzyme of m⁶A modification may have opposite effects on tumorigenesis in different systems, even within one specific type of tumor. For example, Somasundaram et al. found that *METTL3* acts as an oncogene that promotes tumorigenesis, glioblastoma stem cell maintenance, and radio resistance by regulating SRY-Box 2 (*SOX2*) [50], whereas Shi et al. reported opposite effects, including inhibition of tumorigenesis and glioblastoma stem cell self-renewal/proliferation via regulation of ADAM metalloproteinase domain 19 (*ADAM19*) [43]. *METTL14* inhibits tumor invasion and metastasis by regulating *miR-126* [51] while promoting tumor cell proliferation and migration by regulating suppressor of cytokine signaling 2 (*SOCS2*) [41]. In addition, the key enzyme of m⁶A modification could also be involved in other non-m⁶A modification activities. For example, *METTL3* and YTH N⁶-methyladenosine RNA binding protein 3 (YTHDF3) directly regulate translation by cooperating with eukaryotic translation initiation factor 3 (eIF3), independent of m⁶A [52, 53]. Future systematic studies could focus on the detailed mechanism of m⁶A-related proteins regulating tumor fate.

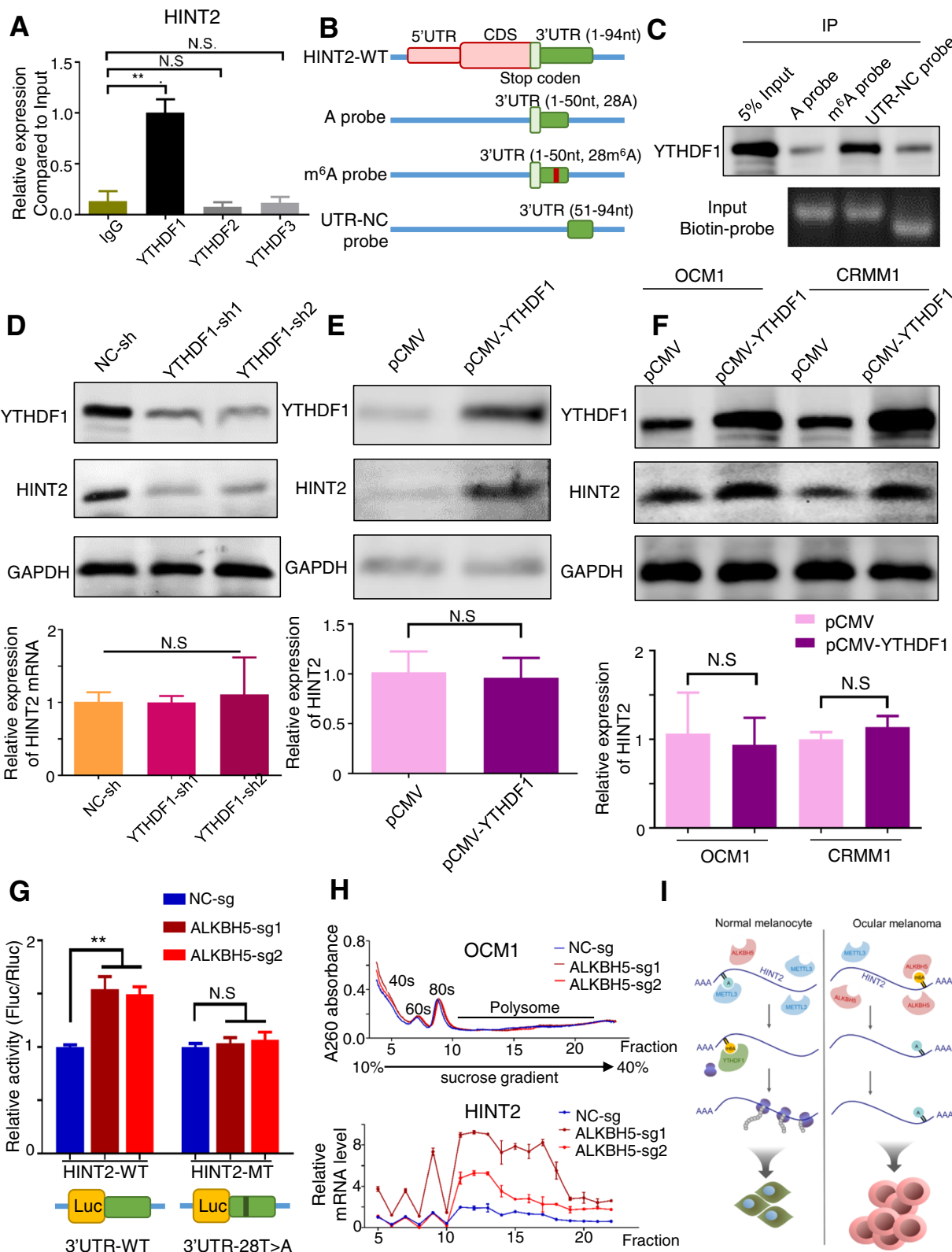


Fig. 7 (See legend on next page.)

(See figure on previous page.)

Fig. 7 YTHDF1 promoted HINT2 translation. **a** Reduction in m⁶A modification at specific regions of *HINT2* transcripts, as assessed by gene-specific YTHDF1, YTHDF2 and YTHDF3 RIP-qPCR assays, in PIG1 cells. The value obtained for the IgG was set to 1. Error bars indicate the mean ± SEM, *n* = 3, ***p* < 0.01. **b** Model showing RNA probes used in RNA pull-down assays. **c** RNA pulldown of endogenous YTHDF1 proteins from HEK293T nuclear extract using synthetic *HINT2* RNA fragments with or without m⁶A modifications. Images are representative of 3 independent experiments. **d** Western blotting (Top) and real-time PCR (Bottom) were performed to elucidate *HINT2* expression in PIG1 cells with or without YTHDF1 knockdown. The *HINT2* and YTHDF1 signals were quantified and normalized to that of *GAPDH*. Error bars indicate the mean ± SEM, *n* = 3. **e, f** Western blotting (Top) and real-time PCR (Bottom) were performed to elucidate *HINT2* expression in PIG1 cells with or without YTHDF1 overexpression. The *HINT2* and YTHDF1 signals were quantified and normalized to that of *GAPDH*. Error bars indicate the mean ± SEM, *n* = 3. **g** Dual luciferase reporter assays showing the effect of ALKBH5 on *HINT2* mRNA reporters with either wild-type or mutated m⁶A sites. Error bars indicate the mean ± SEM, *n* = 3, ****p* < 0.001. **h** Polysome profiling assays. The fractionation of lysates from PIG1 cells with or without *METTL3* knockdown is shown on the top. RNAs in different ribosome fractions were extracted and subjected to qPCR analysis; data are shown on the bottom as the mean ± SD. *n* = 3, **p* < 0.05; ***p* < 0.01; ****p* < 0.001. **i** Model showing how reduced m⁶A methylation alters *HINT2* translation to contribute to tumor progression

m⁶A-modified RNA recognized by different readers could present with different functions. For instance, YTHDF1 mediates nuclear export and translation [10, 54], YTH N⁶-methyladenosine RNA binding protein 2 (YTHDF2) regulates mRNA stability with m⁶A [10, 55] and RNA structural remodeling [33], and YT521-B regulates sex-specific alternative splicing and subcellular localization of mRNAs with m⁶A [56, 57]. Here, we revealed for the first time that the m⁶A modification of *HINT2* is recognized by YTHDF1. Further study could concentrate on the oncogenic role of other readers, such as YTHDF2/3, in regulating tumor formation of ocular melanoma.

HINT2 is a member of the superfamily of histidine triad AMP-lysine hydrolase proteins, which are closely associated with mitochondrial metabolism and tumor suppression [58]. *HINT2* has been reported to expedite Ca²⁺ influx into mitochondria from the cytoplasm, which is a hallmark of the mitochondrial apoptosis pathway and an essential condition for early apoptosis [58]. Loss of *HINT2* disturbs mitochondrial lipid metabolism, glucose homeostasis and mitochondrial deformity [59]. As a tumor suppressor gene, *HINT2* is downregulated in pancreatic cancer and hepatocellular cancer, endometrial cancer and colorectal cancer, preventing the mitochondrial apoptosis pathway and leading to poor survival [38, 39, 60, 61]. Here, we revealed for the first time that *HINT2* is regulated by m⁶A modification, indicating that disturbances in RNA methylation homeostasis result in dysregulation of proliferation and mitochondrial apoptosis, which contributes to the progression of ocular melanoma. Notably, we found that knockdown of *HINT2* only partially rescued the effect of knockdown of *ALKBH5* on ocular melanoma cells, which indicates that there are other cofactors involved in tumorigenesis that are regulated by m⁶A modifications.

Uveal melanoma is the most common adult intraocular tumor, with a 5-year survival rate ranging from 71 to 76% [11]. Additionally, more than half of patients develop metastasis after 5 years [11], and the

median survival time for metastatic UM is only 12 months [62]. Conjunctival melanoma is also a rare but lethal cancer; nearly 30% of patients die within 10 years [63]. Although B-raf mutations are rare in UM, activation changes in other MAPK pathway components, such as *GNAQ* or *GNA11*, are found in 85–95% of patients and are partly responsible for tumorigenesis [64, 65]. In CM, the *B-raf* mutation is present in up to 50% of patients [66]. Ocular melanoma cells with the activated MAPK pathway have been reported to be modestly sensitive to MAPK/ERK kinase (MEK) inhibitors with or without combination treatment with the protein kinase C (PKC) inhibitor [67]. Unfortunately, PKC targeting is limited by toxicity, and a completed phase 3 trial showed no clinical benefit [68]. To date, structure-based selective inhibitors of the m⁶A key enzyme have been discovered [69, 70]. These drugs provide a novel pathway for targeted therapy of ocular melanoma.

Conclusion

In general, we revealed the critical role of m⁶A modification in ocular melanoma tumorigenesis. Decreased m⁶A levels are identified in ocular melanoma samples, indicating poor prognosis, and changes in global m⁶A modification are highly associated with tumor progression. Mechanistically, YTHDF1 promotes the translation of methylated mRNA of *HINT2*, a tumor suppressor in ocular melanoma. Our work uncovers a critical function of m⁶A methylation in ocular melanoma and provides insight into the understanding of m⁶A modification.

Supplementary information

Supplementary information accompanies this paper at <https://doi.org/10.1186/s12943-019-1088-x>.

Additional file 1: Table S1. The clinical characteristics of ocular melanoma patient cohorts in the m⁶A assay.

Additional file 2: Table S2. The clinical characteristics of ocular melanoma patient cohorts in tissue chip.

Additional file 3: Table S3. The detail information of clinical characteristics and gene expression of ocular melanoma patient cohorts in tissue chip.

Additional file 4: Figure S1. m⁶A methylation promoted PIG1 cell proliferation.

Additional file 5: Figure S2. Lower m⁶A methylation promoted ocular melanoma tumorigenesis.

Additional file 6: Figure S3. Higher m⁶A methylation inhibited ocular melanoma tumorigenesis.

Additional file 7: Figure S4. m⁶A-seq of ocular melanoma and normal control cells.

Additional file 8: Figure S5. Characterization and modulation of m⁶A in ocular melanoma cells.

Additional file 9: Table S4. List of protein expression of genes in ocular melanoma cells and normal cells according to the Label-free MS.

Additional file 10: Figure S6. Overexpression of *HINT2* inhibited ocular melanoma tumorigenesis.

Additional file 11: Figure S7. *HINT2* translation was promoted by m⁶A modification.

Additional file 12: Table S5. Oligonucleotides used in this study.

Additional file 13: Table S6. Antibodies used in this study.

Additional file 14: Table S7. Primers used in this study.

Additional file 15. Unprocessed original scans of blots.

Abbreviations

ADAM19: ADAM metalloproteinase domain 19; ALKBH5: α -ketoglutarate-dependent dioxygenase alkB homolog 5; CANT1: LncRNA CASC15-New-Transcript 1; CM: Conjunctival melanoma; eIF3: Eukaryotic translation initiation factor 3; FTO: Fat-mass and obesity-associated protein; GNA11: G protein subunit alpha 11; GNAQ: G protein subunit alpha Q; GSEA: Genome-wide gene set enrichment analysis; HINT2: Histidine triad nucleotide-binding protein 2; m¹A: N¹-methyladenosine; m⁵C: N⁵-methylcytosine; m⁶A: N⁶-methyladenosine; m⁶Am: N⁶,2'-O-dimethyladenosine; MAPK: Mitogen-activated protein kinase; MEK: MAPK/ERK kinase; MeRIP-seq: methylated RNA immunoprecipitation sequencing; METTL14: Methyltransferase-like 14; METTL3: Methyltransferase-like 3; miCLIP-seq: m⁶A individual-nucleotide-resolution cross-linking and immunoprecipitation with sequencing; PKC: Protein kinase C; RIP: RNA-binding protein immunoprecipitation; SOCS2: Suppressor of cytokine signaling 2; SOX2: SRY-box 2; UM: Uveal melanoma; UTR: Untranslated region; WTAP: Wilms tumor associated protein; YTHDF1: YTH N⁶-methyladenosine RNA binding protein 1; YTHDF2: YTH N⁶-methyladenosine RNA binding protein 2; YTHDF3: YTH N⁶-methyladenosine RNA binding protein 3

Acknowledgments

We thank all the uveal melanoma and conjunctival melanoma patients enrolled in our study and wish them good health.

Authors' contributions

XQF and YGY conceived this project and supervised all the experiments. RBJ and PWC designed and performed the molecular biology, protein chemistry, and cell culture experiments. RBJ and PWC analyzed the data and drafted the manuscript. RBJ, YFX and SFG were responsible for sample collection. YY, SZW and BFS performed the m⁶A-seq and bioinformatic analyses with prediction and experimental candidate selection with assistance from RBJ and PWC. All authors read and approved the final manuscript.

Funding

This work was supported by the National Key R&D Program of China (2018YFC1106100, 2018YFC1106101), the National Natural Science Foundation of China (Grant No. 81772875, 81570884, 81770961, 91753000, U1932135), the Research Grant of the Shanghai Science and Technology Committee (17DZ2260100), Shanghai Municipal Science and Technology Major Project (2017SHZDZX01) and the CAS Key Research Projects of Frontier Science (QZYDY-SSW-SMC027).

Availability of data and materials

The raw sequence data reported in this paper, including RNA-seq, miCLIP-seq and MeRIP-seq data, have been deposited in the Gene Expression Omnibus database under accession number GSE137675, and also the Genome Sequence Archive [71] in the BIG Data Center [72], Beijing Institute of Genomics (BIG), Chinese Academy of Sciences, under accession number CRA001675 (<http://bigd.big.ac.cn/gsa/s/n110138p>) and are publicly accessible at <http://bigd.big.ac.cn/gsa>.

Ethics approval and consent to participate

This research was performed in accordance with the World Medical Association Declaration of Helsinki. Written informed consent was obtained from all patients. The study was approved by the Ethics Committee of Shanghai JiaoTong University.

Consent for publication

Not applicable.

Competing interests

The authors declare no competing financial interests.

Author details

¹Department of Ophthalmology, Ninth People's Hospital, Shanghai JiaoTong University School of Medicine, Shanghai 20025, People's Republic of China. ²Key Laboratory of Genomic and Precision Medicine, Collaborative Innovation Center of Genetics and Development, Beijing Institute of Genomics, Chinese Academy of Sciences, Beijing 100101, China. ³Shanghai Key Laboratory of Orbital Diseases and Ocular Oncology, Shanghai 20025, People's Republic of China. ⁴Sino-Danish College, University of Chinese Academy of Sciences, Beijing 100049, China. ⁵Institute for Stem Cell and Regeneration, Chinese Academy of Sciences, Beijing 100101, China.

Received: 8 July 2019 Accepted: 14 October 2019

Published online: 14 November 2019

References

- Roundtree IA, Evans ME, Pan T, He C. Dynamic RNA modifications in gene expression regulation. *Cell*. 2017;169:1187–200.
- Yang Y, Hsu PJ, Chen YS, Yang YG. Dynamic transcriptomic m⁶A decoration: writers, erasers, readers and functions in RNA metabolism. *Cell Res*. 2018;28:616–24.
- Zhang C, Chen Y, Sun B, Wang L, Yang Y, Ma D, Lv J, Heng J, Ding Y, Xue Y, et al. m⁶A modulates haematopoietic stem and progenitor cell specification. *Nature*. 2017;549:273–6.
- Weng H, Huang H, Wu H, Qin X, Zhao BS, Dong L, Shi H, Skibbe J, Shen C, Hu C, et al. METTL14 inhibits hematopoietic stem/progenitor differentiation and promotes Leukemogenesis via mRNA m⁶A modification. *Cell Stem Cell*. 2018;22:191–205 e199.
- Agarwala SD, Blitzblau HG, Hochwagen A, Fink GR. RNA methylation by the MIS complex regulates a cell fate decision in yeast. *PLoS Genet*. 2012;8:e1002732.
- Jia G, Fu Y, Zhao X, Dai Q, Zheng G, Yang Y, Yi C, Lindahl T, Pan T, Yang YG, He C. N⁶-methyladenosine in nuclear RNA is a major substrate of the obesity-associated FTO. *Nat Chem Biol*. 2011;7:885–7.
- Zhang S, Zhao BS, Zhou A, Lin K, Zheng S, Lu Z, Chen Y, Sulman EP, Xie K, Bogler O, et al. m⁶A Demethylase ALKBH5 maintains Tumorigenicity of Glioblastoma stem-like cells by sustaining FOXM1 expression and cell proliferation program. *Cancer Cell*. 2017;31:591–606 e596.
- Zhang Z, Wang M, Xie D, Huang Z, Zhang L, Yang Y, Ma D, Li W, Zhou Q, Yang YG, Wang XJ. METTL3-mediated N⁶-methyladenosine mRNA modification enhances long-term memory consolidation. *Cell Res*. 2018;28:1050–61.
- Wang S, Chai P, Jia R, Jia R. Novel insights on m⁶A RNA methylation in tumorigenesis: a double-edged sword. *Mol Cancer*. 2018;17:101.
- Liu J, Eckert MA, Harada BT, Liu SM, Lu Z, Yu K, Tienda SM, Chryplewicz A, Zhu AC, Yang Y, et al. m⁶A mRNA methylation regulates AKT activity to promote the proliferation and tumorigenicity of endometrial cancer. *Nat Cell Biol*. 2018;20:1074–83.
- Kujala E, Makitie T, Kivela T. Very long-term prognosis of patients with malignant uveal melanoma. *Invest Ophthalmol Vis Sci*. 2003;44:4651–9.

12. Shields CL, Markowitz JS, Belinsky I, Schwartzstein H, George NS, Lally SE, Mashayekhi A, Shields JA. Conjunctival melanoma: outcomes based on tumor origin in 382 consecutive cases. *Ophthalmology*. 2011;118:389–95 e381–382.
13. Shields CL. Conjunctival melanoma: risk factors for recurrence, exenteration, metastasis, and death in 150 consecutive patients. *Trans Am Ophthalmol Soc*. 2000;98:471–92.
14. Larsen AC. Conjunctival malignant melanoma in Denmark. Epidemiology, treatment and prognosis with special emphasis on tumorigenesis and genetic profile. *Acta Ophthalmol*. 2016;94:842.
15. Xing Y, Wen X, Ding X, Fan J, Chai P, Jia R, Ge S, Qian G, Zhang H, Fan X. CANT1 lncRNA triggers efficient therapeutic efficacy by correcting aberrant lncRNA cascade in malignant uveal melanoma. *Mol Ther*. 2017;25:1209–21.
16. Sharma A, Stei MM, Frohlich H, Holz FG, Loeffler KU, Herwig-Carl MC. Genetic and epigenetic insights into uveal melanoma. *Clin Genet*. 2018;93:952–61.
17. Dominissini D, Moshitch-Moshkovitz S, Salmon-Divon M, Amariglio N, Rechavi G. Transcriptome-wide mapping of N⁶-methyladenosine by m⁶A-seq based on immunocapturing and massively parallel sequencing. *Nat Protoc*. 2013;8:176–89.
18. Martin M. Cutadapt removes adapter sequences from high-throughput sequencing reads. *EMBnet J*. 2011;17:10.
19. Bolger AM, Lohse M, Usadel B. Trimmomatic: a flexible trimmer for Illumina sequence data. *Bioinformatics*. 2014;30:2114–20.
20. Kim D, Langmead B, Salzberg SL. HISAT: a fast spliced aligner with low memory requirements. *Nat Methods*. 2015;12:357–60.
21. Zhang Y, Liu T, Meyer CA, Eeckhoutte J, Johnson DS, Bernstein BE, Nusbaum C, Myers RM, Brown M, Li W, Liu XS. Model-based analysis of ChIP-Seq (MACS). *Genome Biol*. 2008;9:R137.
22. Quinlan AR, Hall IM. BEDTools: a flexible suite of utilities for comparing genomic features. *Bioinformatics*. 2010;26:841–2.
23. Liao Y, Smyth GK, Shi W. Feature counts: an efficient general purpose program for assigning sequence reads to genomic features. *Bioinformatics*. 2014;30:923–30.
24. Love MI, Huber W, Anders S. Moderated estimation of fold change and dispersion for RNA-seq data with DESeq2. *Genome Biol*. 2014;15:550.
25. Moore MJ, Zhang C, Gantman EC, Mele A, Darnell JC, Darnell RB. Mapping Argonaute and conventional RNA-binding protein interactions with RNA at single-nucleotide resolution using HITS-CLIP and CIMS analysis. *Nat Protoc*. 2014;9:263–93.
26. Shah A, Qian Y, Weyn-Vanhenhenryck SM, Zhang C. CLIP tool kit (CTK): a flexible and robust pipeline to analyze CLIP sequencing data. *Bioinformatics*. 2017;33:566–7.
27. Li H, Durbin R. Fast and accurate short read alignment with burrows-wheeler transform. *Bioinformatics*. 2009;25:1754–60.
28. Linder B, Grozhik AV, Olarerin-George AO, Meydan C, Mason CE, Jaffrey SR. Single-nucleotide-resolution mapping of m⁶A and m⁶Am throughout the transcriptome. *Nat Methods*. 2015;12:767–72.
29. Weyn-Vanhenhenryck SM, Mele A, Yan Q, Sun S, Farny N, Zhang Z, Xue C, Herre M, Silver PA, Zhang MQ, et al. HITS-CLIP and integrative modeling define the Rbfox splicing-regulatory network linked to brain development and autism. *Cell Rep*. 2014;6:1139–52.
30. Vu LP, Pickering BF, Cheng Y, Zaccara S, Nguyen D, Minuesa G, Chou T, Chow A, Saletore Y, MacKay M, et al. The N⁶-methyladenosine (m⁶A)-forming enzyme METTL3 controls myeloid differentiation of normal hematopoietic and leukemia cells. *Nat Med*. 2017;23:1369–76.
31. Heinz S, Benner C, Spann N, Bertolino E, Lin YC, Laslo P, Cheng JX, Murre C, Singh H, Glass CK. Simple combinations of lineage-determining transcription factors prime cis-regulatory elements required for macrophage and B cell identities. *Mol Cell*. 2010;38:576–89.
32. Wang Z, Yang B, Zhang M, Guo W, Wu Z, Wang Y, Jia L, Li S. Cancer genome atlas research N, Xie W, Yang D: lncRNA epigenetic landscape analysis identifies EPIC1 as an oncogenic lncRNA that interacts with MYC and promotes cell-cycle progression in Cancer. *Cancer Cell* 2018, 33:706–720 e709.
33. Liu N, Dai Q, Zheng G, He C, Parisien M, Pan T. N⁶-methyladenosine-dependent RNA structural switches regulate RNA-protein interactions. *Nature*. 2015;518:560–4.
34. Hsu PJ, Zhu Y, Ma H, Guo Y, Shi X, Liu Y, Qi M, Lu Z, Shi H, Wang J, et al. Ythdc2 is an N⁶-methyladenosine binding protein that regulates mammalian spermatogenesis. *Cell Res*. 2017;27:1115–27.
35. Yang X, Yang Y, Sun BF, Chen YS, Xu JW, Lai WY, Li A, Wang X, Bhattarai DP, Xiao W, et al. 5-methylcytosine promotes mRNA export - NSUN2 as the methyltransferase and ALYREF as an m⁵C reader. *Cell Res*. 2017;27:606–25.
36. Huang H, Weng H, Sun W, Qin X, Shi H, Wu H, Zhao BS, Mesquita A, Liu C, Yuan CL, et al. Recognition of RNA N⁶-methyladenosine by IGF2BP proteins enhances mRNA stability and translation. *Nat Cell Biol*. 2018;20:285–95.
37. Lence T, Akhtar J, Bayer M, Schmid K, Spindler L, Ho CH, Kreim N, Andrade-Navarro MA, Poeck B, Helm M, Roignant JY. m⁶A modulates neuronal functions and sex determination in *Drosophila*. *Nature*. 2016;540:242–7.
38. Chen L, Sun Q, Zhou D, Song W, Yang Q, Ju B, Zhang L, Xie H, Zhou L, Hu Z, et al. HINT2 triggers mitochondrial Ca²⁺ influx by regulating the mitochondrial Ca²⁺ uniporter (MCU) complex and enhances gemcitabine apoptotic effect in pancreatic cancer. *Cancer Lett*. 2017;411:106–16.
39. Martin J, Magnino F, Schmidt K, Piguat AC, Lee JS, Semela D, St-Pierre MV, Ziemięcki A, Cassio D, Brenner C, et al. HINT2, a mitochondrial apoptotic sensitizer down-regulated in hepatocellular carcinoma. *Gastroenterology*. 2006;130:2179–88.
40. Barbieri I, Tzelepis K, Pandolfini L, Shi J, Millan-Zambrano G, Robson SC, Aspris D, Migliori V, Bannister AJ, Han N, et al. Promoter-bound METTL3 maintains myeloid leukaemia by m⁶A-dependent translation control. *Nature*. 2017;552:126–31.
41. Chen M, Wei L, Law CT, Tsang FH, Shen J, Cheng CL, Tsang LH, Ho DW, Chiu DK, Lee JM, et al. RNA N⁶-methyladenosine methyltransferase-like 3 promotes liver cancer progression through YTHDF2-dependent posttranscriptional silencing of SOCS2. *Hepatology*. 2018;67:2254–70.
42. Li Z, Weng H, Su R, Weng X, Zuo Z, Li C, Huang H, Nachtergaele S, Dong L, Hu C, et al. FTO plays an oncogenic role in acute myeloid leukemia as a N⁶-Methyladenosine RNA Demethylase. *Cancer Cell*. 2017;31:127–41.
43. Cui Q, Shi H, Ye P, Li L, Qu Q, Sun G, Sun G, Lu Z, Huang Y, Yang CG, et al. m⁶A RNA methylation regulates the self-renewal and tumorigenesis of Glioblastoma stem cells. *Cell Rep*. 2017;18:2622–34.
44. Zhang J, Bai R, Li M, Ye H, Wu C, Wang C, Li S, Tan L, Mai D, Li G, et al. Excessive miR-25-3p maturation via N⁶-methyladenosine stimulated by cigarette smoke promotes pancreatic cancer progression. *Nat Commun*. 2019;10:1858.
45. Zhang C, Zhang M, Ge S, Huang W, Lin X, Gao J, Gong J, Shen L. Reduced m⁶A modification predicts malignant phenotypes and augmented Wnt/PI3K-Akt signaling in gastric cancer. *Cancer Med*. 2019;8:4766–81.
46. Zhu H, Gan X, Jiang X, Diao S, Wu H, Hu J. ALKBH5 inhibited autophagy of epithelial ovarian cancer through miR-7 and BCL-2. *J Exp Clin Cancer Res*. 2019;38:163.
47. Peng W, Li J, Chen R, Gu Q, Yang P, Qian W, Ji D, Wang Q, Zhang Z, Tang J, Sun Y. Upregulated METTL3 promotes metastasis of colorectal Cancer via miR-1246/SPRED2/MAPK signaling pathway. *J Exp Clin Cancer Res*. 2019;38:393.
48. Feng Z, Li Q, Meng R, Yi B, Xu Q. METTL3 regulates alternative splicing of MyD88 upon the lipopolysaccharide-induced inflammatory response in human dental pulp cells. *J Cell Mol Med*. 2018;22:2558–68.
49. Lin S, Choe J, Du P, Triboulet R, Gregory RI. The m⁶A methyltransferase METTL3 promotes translation in human Cancer cells. *Mol Cell*. 2016;62:335–45.
50. Visvanathan A, Patil V, Arora A, Hegde AS, Arivazhagan A, Santosh V, Somasundaram K. Essential role of METTL3-mediated m⁶A modification in glioma stem-like cells maintenance and radioresistance. *Oncogene*. 2018;37:522–33.
51. Ma JZ, Yang F, Zhou CC, Liu F, Yuan JH, Wang F, Wang TT, Xu QG, Zhou WP, Sun SH. METTL14 suppresses the metastatic potential of hepatocellular carcinoma by modulating N⁶-methyladenosine-dependent primary MicroRNA processing. *Hepatology*. 2017;65:529–43.
52. Choe J, Lin S, Zhang W, Liu Q, Wang L, Ramirez-Moya J, Du P, Kim W, Tang S, Sliz P, et al. mRNA circularization by METTL3-elf3h enhances translation and promotes oncogenesis. *Nature*. 2018;561:556–60.
53. Shi H, Wang X, Lu Z, Zhao BS, Ma H, Hsu PJ, Liu C, He C. YTHDF3 facilitates translation and decay of N⁶-methyladenosine-modified RNA. *Cell Res*. 2017;27:315–28.
54. Roundtree IA, Luo GZ, Zhang Z, Wang X, Zhou T, Cui Y, Sha J, Huang X, Guerrero I, Xie P, et al. YTHDC1 mediates nuclear export of N⁶-methyladenosine methylated mRNAs. *Elife*. 2017;6.
55. Wang X, Lu Z, Gomez A, Hon GC, Yue Y, Han D, Fu Y, Parisien M, Dai Q, Jia G, et al. N⁶-methyladenosine-dependent regulation of messenger RNA stability. *Nature*. 2014;505:117–20.

56. Haussmann IU, Bodi Z, Sanchez-Moran E, Mongan NP, Archer N, Fray RG, Soller M. m⁶A potentiates Sxl alternative pre-mRNA splicing for robust *Drosophila* sex determination. *Nature*. 2016;540:301–4.
57. Fustin JM, Doi M, Yamaguchi Y, Hida H, Nishimura S, Yoshida M, Isagawa T, Morioka MS, Kakeya H, Manabe I, Okamura H. RNA-methylation-dependent RNA processing controls the speed of the circadian clock. *Cell*. 2013;155:793–806.
58. Ndiaye D, Collado-Hilly M, Martin J, Prigent S, Dufour JF, Combettes L, Dupont G. Characterization of the effect of the mitochondrial protein Hint2 on intracellular Ca²⁺ dynamics. *Biophys J*. 2013;105:1268–75.
59. Martin J, Maurhofer O, Bellance N, Benard G, Graber F, Hahn D, Galinier A, Hora C, Gupta A, Ferrand G, et al. Disruption of the histidine triad nucleotide-binding hint2 gene in mice affects glycemic control and mitochondrial function. *Hepatology*. 2013;57:2037–48.
60. Lee LR, Teng PN, Nguyen H, Hood BL, Kavandi L, Wang G, Turbov JM, Thaete LG, Hamilton CA, Maxwell GL, et al. Progesterone enhances calcitriol antitumor activity by upregulating vitamin D receptor expression and promoting apoptosis in endometrial cancer cells. *Cancer Prev Res (Phila)*. 2013;6:731–43.
61. Li W, Cai S, Wang L, Yang C, Zhou B, Wang H. HINT2 downregulation promotes colorectal carcinoma migration and metastasis. *Oncotarget*. 2017;8:13521–31.
62. Rietschel P, Panageas KS, Hanlon C, Patel A, Abramson DH, Chapman PB. Variates of survival in metastatic uveal melanoma. *J Clin Oncol*. 2005;23:8076–80.
63. Satchi K, McKelvie P, McNab AA. Malignant melanoma of the lacrimal drainage apparatus complicating conjunctival melanoma. *Ophthalmic Plast Reconstr Surg*. 2015;31:207–10.
64. Yang J, Manson DK, Marr BP, Carvajal RD. Treatment of uveal melanoma: where are we now? *Ther Adv Med Oncol*. 2018;10:1758834018757175.
65. Field MG, Harbour JW. Recent developments in prognostic and predictive testing in uveal melanoma. *Curr Opin Ophthalmol*. 2014;25:234–9.
66. Larsen AC, Dahmcke CM, Dahl C, Siersma VD, Toft PB, Coupland SE, Prause JU, Guldberg P, Heegaard S. A retrospective review of Conjunctival melanoma presentation, treatment, and outcome and an investigation of features associated with BRAF mutations. *JAMA Ophthalmol*. 2015;133:1295–303.
67. Chen X, Wu Q, Tan L, Porter D, Jager MJ, Emery C, Bastian BC. Combined PKC and MEK inhibition in uveal melanoma with GNAQ and GNA11 mutations. *Oncogene*. 2014;33:4724–34.
68. Komatsubara KM, Manson DK, Carvajal RD. Selumetinib for the treatment of metastatic uveal melanoma: past and future perspectives. *Future Oncol*. 2016;12:1331–44.
69. Su R, Dong L, Li C, Nachtergaele S, Wunderlich M, Qing Y, Deng X, Wang Y, Weng X, Hu C, et al. R-2HG exhibits anti-tumor activity by targeting FTO/m⁶A/MYC/CEBPA signaling. *Cell*. 2018;172:90–105 e123.
70. Niu Y, Wan A, Lin Z, Lu X, Wan G. N⁶-Methyladenosine modification: a novel pharmacological target for anti-cancer drug development. *Acta Pharm Sin B*. 2018;8:833–43.
71. Zhang SS, Chen TT, Zhu JW, Zhou Q, Chen X, Wang YQ, Zhao WM. GSA: genome sequence archive. *Yi Chuan*. 2018;40:1044–7.
72. Members BIGDC. The BIG data center: from deposition to integration to translation. *Nucleic Acids Res*. 2017;45:D18–24.

Publisher's Note

Springer Nature remains neutral with regard to jurisdictional claims in published maps and institutional affiliations.

Ready to submit your research? Choose BMC and benefit from:

- fast, convenient online submission
- thorough peer review by experienced researchers in your field
- rapid publication on acceptance
- support for research data, including large and complex data types
- gold Open Access which fosters wider collaboration and increased citations
- maximum visibility for your research: over 100M website views per year

At BMC, research is always in progress.

Learn more biomedcentral.com/submissions

